Computing the dynamics of biomembranes by combining conservative level set and adaptive finite element methods

Aymen Laadhari, Pierre Saramito, Chaouqi Misbah

Computing the dynamics of biomembranes by combining conservative level set and adaptive finite element methods

Aymen Laadhari, Pierre Saramito and Chaouqi Misbah

January 22, 2013

Abstract – The numerical simulation of the deformation of vesicle membranes under simple shear external fluid flow is considered in this paper. A new saddle-point approach is proposed for the imposition of the fluid incompressibility and the membrane inextensibility constraints, through Lagrange multipliers defined in the fluid and on the membrane respectively. Using a level set formulation, the problem is approximated by mixed finite elements combined with an automatic adaptive mesh procedure at the vicinity of the membrane boundary. Numerical experiments show that this combination of the saddle-point and adaptive mesh method enhances the robustness of the method. The effect of inertia on the stability of the vesicle in a shear flow is also investigated.

Keyword: level set method ; mass conservation ; adaptive finite element method ; Helfrich energy ; vesicle dynamics ; fluid mechanics.

1 Introduction

Phospholipid membranes are abundant in biology. They represent the major component of the cytoplasmic membrane of real cells. They are also present within the cell cytoplasm, e.g. the Golgi apparatus, a complex assembly of phospholipid layers which serve to form small vesicles for protein transport. Phospholipid membranes are also used in many industrial applications, as in giant liposome emulsions for cosmetics. A simple closed membrane of pure phospholipid suspended in an aqueous solution, also called a suspension of *vesicles*, constitute an attractive model system in order to describe mechanical and viscoelastic behaviors of many cells, like red blood cells. They are also considered as promising

drug carriers for a delivery at specific sites in the organisms. This explains the increasing interest for biological membranes from various communities ranging from biology [53, 47] to applied mathematics [50, 29, 6]. This contribution is concerned with a certain aspect of mathematical modeling of vesicles, and more generally of phospholipid membranes.

Vesicles are formed by amphiphilic molecules self-assembled in water to build bilayers, in a certain range of concentration and temperature. At room, as well as at the physiological temperature, the membrane is a two dimensional incompressible fluid. Due to incompressibility, the main mode of deformation of a vesicle is bending. A basic ingredient for biomembranes is thus bending energy. Canham [13] and Helfrich [25, 42] introduced the following expression of the bending energy:

$$\frac{k}{2}\int_\Gamma (H - H_0)^2 \,\mathrm{d}s + \frac{k_g}{2}\int_\Gamma K \,\mathrm{d}s, \tag{1}$$

where $H = H_1 + H_2$ is the mean curvature of the membrane surface, with H_1 and H_2 are the principle curvatures and $K = H_1 H_2$ is the Gauss curvature. The membrane surface is denoted by Γ while Ω represents the volume inside the vesicle, such that $\Gamma = \partial\Omega$. The integrals are performed along the membrane surface where $\mathrm{d}s$ denotes a surface area, while, in this paper, $\mathrm{d}x$ will represent a volume element. The constants k and k_g have the dimension of an energy and represent the bending modulus and the Gaussian curvature modulus, respectively. Here, H_0 denotes the spontaneous curvature that describes the asymmetry of the membrane. In this paper, $H_0 = 0$, since H_0 is relevant only for three-dimensional problems (see appendix A) and we restrict ourself to the bidimensional case in this paper. Finally, from the Gauss-Bonnet theorem, the second term of the Canham-Helfrich energy (1) is a topological invariant. Since topological changes are not considered in this paper, this second term is omitted.

Vesicles can be more or less inflated. The deflation could be due to osmotic effects, depending on additives in the solution. It could also be due to thermal effects: the thermal expansion of phospholipids is greater than those of the water inside the membrane, and thus, the area A_0 of the vesicle increases more rapidly than its volume V_0. The *reduced volume*, denoted by γ, measures the deflation:

$$\gamma = \frac{3V_0}{4\pi} \times \left(\frac{4\pi}{A_0}\right)^{3/2} \in]0, 1]. \tag{2}$$

Thus, γ compares the vesicle volume V_0 with the volume of a sphere having the area equal to A_0: γ is a dimensionless number, that equals to 1 when the vesicle is a sphere and is lower than 1 otherwise. For instance, for the human red blood cell $\gamma \approx 0.64$. By varying γ, the shape that minimizes the energy of curvature can vary from an ellipsoid stretched to a biconcave shape, towards forms varied as that of the Peanut. In the two-dimensional case, V_0 and A_0 denotes the area

and the perimeter respectively. The reduced area γ compares the area of the vesicle with the area of a circle having the same perimeter as the vesicle. The reduced area is expressed in the two-dimensional case by:

$$\gamma \;=\; \frac{V_0}{\pi} \times \left(\frac{2\pi}{A_0}\right)^2 .$$

Remark that, for a circle, the reduced area equals to 1. As the vesicle membrane is impermeable (no osmosis), the number of molecules remains fixed in each layer, and the energetic cost of stretching or compressing the membrane is much larger than the cost of bending deformations: the membrane could be considered as inextensible. In order to satisfy this inextensibility constraint, two approaches are commonly available. The first one use the penalty approach, together with a penalty parameter (see e.g. [15, 18]): the inextensibility constraint then is not exactly satisfied and the approximate solution depends upon the penalty parameter. Recently, Kim and al. [32] proposed a penalty immersed boundary method to simulate the dynamics of inextensible vesicle. In this sence, a virtual force is introduced in order to take into account the inextensibility constraint. The second solution introduces a Lagrange multiplier, that interprets as the surface tension of the membrane, and the inextensibility constraints is exactly satisfied. In the present work, the second solution was selected, since it avoids the dependence of the solution upon the penalty parameter. This formulation based on Lagrange multipliers is of common use for incompressible fluid flow applications (see e.g. [49]).

Furthermore, for general interface fluid flow problems, there are two main classes of numerical methods usually used: the class of Lagrangian methods based on an explicit interface parameterization and discretization while the class of Eulerian methods uses an implicit function. The popular phase field and level set methods fall into this second class.

For Lagrangian methods, the interface, which represents here the biological membrane, is discretized by a set of points which are moved with a speed depending on the studied problem. For the computation of static vesicle shapes, the *classical finite element method* has been extensively used for surface restauration problems [4]. In [46, 14] the authors proposed a semi-implicit variational formulation (see also [28] for another semi-implicit approach in the context of capillary problems). In [39], an augmented Lagrangian algorithm was introduced in order to enforce the volume and area conservation while computing the static shape of a vesicle. In [9], the volume and area conservation constraints was enforced at the discrete level to machine precision. For the dynamic of vesicles in interaction with a fluid, the mesh, capturing the interface, may regenerated at each time step, while the boundary conditions between inside and outside volume of the interface could be directly imposed on this explicit boundary. The older method used for vesicle fluid applications falls into this category: the *boundary element method*

transforms all viscous volume terms into surface integrals through a Green kernel and only a surface mesh of the interface is required [44] (see also [45, 8]). Nevertheless, inertia terms are not reducible to boundary integrals and, despite some recent improvements, this approach suffers from some limitations. A more recent approach bases on both a mesh of the interface and a volume mesh. When the volume mesh is compatible with the interface discretization, the *classical finite element method* could be used [12]. A commonly used variant fixes the volume mesh one time for all and expresses interface integrals on a discrete moving surface mesh: this is the so called *penalty immersed boundary method* [32, 34].

The Eulerian methods are characterized by the use of a meshing strategy that is independent of the movements of the interface: this approach allows the use of fixed and fully structured volume mesh. Moreover, no more surface mesh of the moving interface is required. Very complex shapes, with strong variations of the curvature and possible topological changes becomes possible. In the case of a diffuse interface, as for fluid mixtures, the interface is represented by a smooth transition zone. Indeed, at least at the molecular scale, there is a small zone of mixture between species. From a numerical point of view, the diffuse interface notion could be interpreted as a way of regularization of a sharp interface, together with a regularization parameter, associated to the interface width: this is the *phase field method*, introduced by Allen and Cahn [2], and applied recently to vesicles [19] and their fluid interactions [7, 17]. A second Eulerian method, the *level set method* [41], do no more requires any regularization and is able to catch sharp interfaces: a simple transport equation is used to move the level set function. See [40, 16] for recent applications to vesicle dynamics.

Nevertheless, both phase field and level set methods suffer a lack of precision when dealing with the volume and area conservation constraints. The aim of this paper is to present a new level set method that exactly solve these constraints at the discrete level at machine precision: it extends to the vesicle dynamics a previous work on level set methods for the advection equation [36].

We focus our attention on describing the dynamics of a single suspended vesicle in a linear shear gradient of a plane flow. Vesicles in shear flow in the limit of the vanishing Reynolds number (also called the Stokes limit) have been the subject of extensive studies [6]. Few works deals with the effect of fluid inertia on the dynamics of the vesicle: let us mention the pioneers works of [48] and [38] that both observe a variation of inclination the angle of the vesicle under a shear flow when the Reynolds number increases. In the present work, non-zero Reynolds numbers are considered and the effect of inertia are more deeply investigated. This situation is of practical interest for red blood cells applications.

The outline of the paper is as follows. A saddle-point approach allows us to characterize the solution in a weak formulation, which is discretized using mixed finite elements in section 2. In Section 3 we focus on the numerical method. We

present our level set method formulation for the vesicle dynamics and show the finite element discretization as well the advection mass preservation improvement. Section 4 is devoted to show numerical results illustrating the vesicle membrane in the tumbling and the tank-treading regimes. Finally, the effect of the inertia terms is explorated and we show that, beyond a critical value of the Reynolds number, the vesicle passes from a tumbling to a tank-treading regime.

2 Problem statement

2.1 Notations and preliminary results

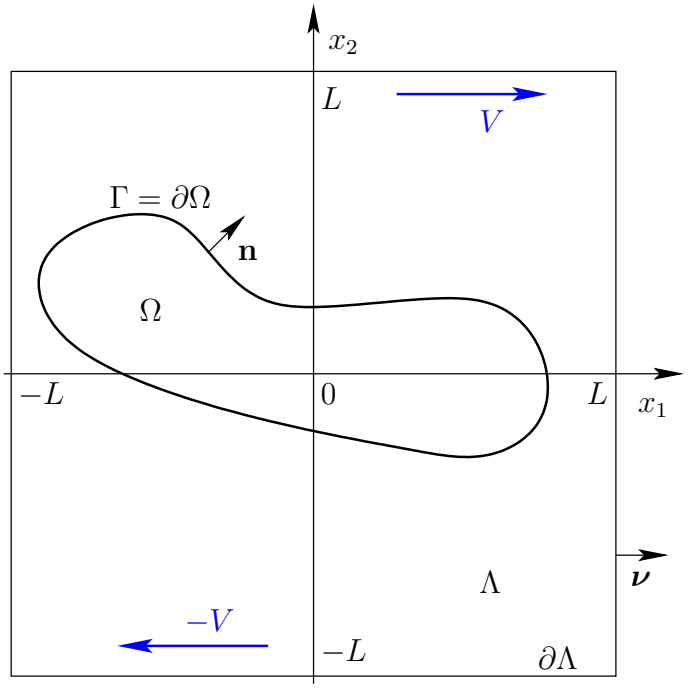

Figure 1: Notations for the vesicle interacting with a surrounding shear flow.

Let $\Lambda =]-L, L[^d$ be the bounded region containing the vesicle and the surrounding fluid, where $L > 0$ is the half domain width. Numerical computations are performed in this paper with $d = 2$, while the mathematical formulation could be extended to $d = 3$ with few modifications. Let $T > 0$: for any $t \in]0, T[$, the membrane $\Gamma(t) \subset \Lambda$ is the closed surface defined by:

$$\Gamma(t) = \{(t, x) \in]0, T[\times\Lambda; \quad \phi(t, x) = 0\}, \tag{3}$$

where ϕ is the level set function. By convention, the vesicle $\Omega(t) \subset \Lambda$ is the region where $\phi(t, .)$ is negative and we have $\Gamma(t) = \partial\Omega(t)$.

Let $\mathbf{u}$ denote the velocity of the fluid in Λ. The membrane $\Gamma(t)$ is transported at the same velocity, and thus, the level set function satisfies:

$$\frac{D\phi}{Dt} = \frac{\partial \phi}{\partial t} + \mathbf{u}.\nabla\phi = 0 \quad \text{in} \quad]0,T[\times\Lambda, \tag{4a}$$

where D/Dt denotes the material derivative. The previous transport equation may be completed by suitable boundary and initial conditions:

$$\begin{aligned} \phi &= \phi_b \quad \text{on} \quad]0,T[\times\Sigma_- & \text{(4b)} \\ \phi(0) &= \phi_0 \quad \text{in} \quad \Lambda & \text{(4c)} \end{aligned}$$

where $\Sigma_- = \{x \in \partial\Lambda;\ \mathbf{u}.\boldsymbol{\nu}(x) < 0\}$ is the upstream and $\boldsymbol{\nu}$ denotes the outward unit normal to the surrounding bounding box Λ. Concerning the initial condition (4c), the function ϕ_0 denotes the *signed distance* between x and the given initial shape membrane $\partial\Omega(0)$:

$$\phi_0(x) = \begin{cases} \inf\{|y-x|;\ y \in \partial\Omega(0)\} & \text{when } x \notin \Omega(0), \\ \inf\{-|y-x|;\ y \in \partial\Omega(0)\} & \text{otherwise.} \end{cases}$$

Let $\mathbf{n}$ denote the unit outward normal vector to the shape Ω (see Fig. 1). Let f be any scalar function and $\mathbf{v}$ be any vector field. The surface gradient, the surface divergence and the Laplace-Beltrami operator are respectively expressed by:

$$\begin{aligned} \nabla_s f &= (I - \mathbf{n}\otimes\mathbf{n})\,\nabla f = \nabla f - (\mathbf{n}.\nabla f)\,\mathbf{n}, & \text{(5a)} \\ \operatorname{div}_s \mathbf{v} &= (I - \mathbf{n}\otimes\mathbf{n}) : \nabla\mathbf{v} = \operatorname{div}\mathbf{v} - ((\nabla\mathbf{v}).\mathbf{n}).\mathbf{n}, & \text{(5b)} \\ \Delta_s f &= \operatorname{div}_s(\nabla_s f)\,. & \text{(5c)} \end{aligned}$$

Here, $\otimes$ denotes the tensorial product of two vectors and the semicolon : is the two times contracted product between tensors.

The mean and the Gauss curvatures can be expressed in terms of the normal $\mathbf{n}$ (see [35]):

$$\begin{aligned} H &= \nabla_s.\mathbf{n} = \nabla.\mathbf{n}, \\ 2K &= H^2 - \nabla\mathbf{n} : \nabla\mathbf{n}^T. \end{aligned}$$

2.2 The dimensional problem

The problem writes:

find ϕ, $\mathbf{u}$, p *and* λ *such that*

$$\frac{\partial \phi}{\partial t} + \mathbf{u}.\nabla\phi = 0 \quad \text{in }]0,T[\times\Lambda \tag{6a}$$

$$\rho\left(\frac{\partial \mathbf{u}}{\partial t} + \mathbf{u}.\nabla\mathbf{u}\right) - \mathbf{div}\left(2\eta\, D(\mathbf{u})\right) + \nabla p = 0 \quad \text{in }]0,T[\times(\Lambda\backslash\partial\Omega) \tag{6b}$$

$$\operatorname{div}\mathbf{u} = 0 \quad \text{in }]0,T[\times\Lambda \tag{6c}$$

$$\operatorname{div}_s\mathbf{u} = 0 \quad \text{on }]0,T[\times\partial\Omega \tag{6d}$$

$$[\mathbf{u}] = 0 \quad \text{on }]0,T[\times\partial\Omega \tag{6e}$$

$$-k\left\{\Delta_s H + H\left(\frac{H^2}{2} - 2K\right)\right\}\mathbf{n} + H\,\lambda\,\mathbf{n} - \nabla_s\lambda + \left[2\eta\, D(\mathbf{u}) - pI\right].\mathbf{n} = 0 \quad \text{on }]0,T[\times\partial\Omega \tag{6f}$$

$$\phi = \phi_b \quad \text{on }]0,T[\times\Sigma_- \tag{6g}$$

$$\mathbf{u} = \mathbf{u}_b \quad \text{on }]0,T[\times\Sigma_D \tag{6h}$$

$$(2\eta D(\mathbf{u}) - pI).\boldsymbol{\nu} = 0 \quad \text{on }]0,T[\times\Sigma_N \tag{6i}$$

$$\phi(0) = \phi_0 \quad \text{in } \Lambda \tag{6j}$$

$$\mathbf{u}(0) = \mathbf{u}_0 \quad \text{in } \Lambda \tag{6k}$$

Equation (6a) expresses that the interface is transported by the fluid. Notice that the conservation of momentum (6b) is written in $\Lambda\backslash\partial\Omega$, i.e. in Ω and its complementary $\Lambda\backslash\overline{\Omega}$. Here, $D(\mathbf{u}) = (\nabla\mathbf{u} + (\nabla\mathbf{u})^T)/2$ is the symmetric part of the gradient of velocity tensor. The viscosity η is not constant over Λ: it takes a constant value η_0 outside the vesicle $\Omega(t)$ and a different constant value η_1 inside the vesicle.

The unknown velocity field may satisfy two constraints: the fluid mass conservation (6c) and the membrane inextensibility (6d). The mass conservation reduces to the divergence-free condition $\operatorname{div}\mathbf{u} = 0$ since the density, denoted by ρ, is supposed to be constant. Conversely, the membrane inextensibility writes locally $\operatorname{div}_s\mathbf{u} = 0$.

On $\partial\Omega$, [.] denotes the jump of a quantity across $\partial\Omega$ in the normal direction $\mathbf{n}$. Equation (6e) expresses the continuity of the velocity across the interface. The jump term in (6f) expresses the balance with membrane strengths. Indeed, the first normal term comes from the Canham-Helfrich bending energy (1) and is not an obvious computation (see [42, 35]), since $\partial\Omega(t)$ and H depend implicitly upon $\mathbf{u}$: it requires some advanced shape optimization tools. This bending energy being a purely geometrical quantity, it cannot give rise to a tangential strength: any tangential movement of points on a surface is only modifying their positions without affecting the shape of the surface and its curvature energy. The second and third terms in (6f) involves the Lagrange multiplier λ (the surface tension), and defined on the membrane $\partial\Omega(t)$. The second term is normal and it is similar

to the strengths of capillarities engendered by the surface tension when modeling of the dynamics of drops. The term $\nabla_s \lambda$ is tangential and its action is known as the Marangoni effect.

The unknown level set ϕ and velocity field $\mathbf{u}$ satisfy some boundary and initial conditions.

The boundary $\Sigma_D =]-L, L[^{d-1} \times \{-L, L\}$ is associated to the Dirichlet boundary condition $\mathbf{u}_b(t, x)$, expressed for a shear flow by:

$$\mathbf{u}_b(t, x) = \begin{cases} V & \text{when } x_d = L \\ -V & \text{when } x_d = -L \end{cases}$$

for all $(t, x) \in]0, T[\times \Sigma_D$. Here, V denotes the given shear velocity at the box boundary (see Fig. 1). Conversely, $\Sigma_N = \{-L, L\}^{d-1} \times]-L, L[$ is associated to a Neumann-type boundary condition.

2.3 Dimensionless problem

The characteristic length R_0 of the vesicle is chosen equal to the radius of a sphere having the same surface as the vesicle $\partial\Omega$ in the tree dimensional case. In the two-dimensional case, it represents the radius of a circle having the same perimeter as $\partial\Omega$. The characteristic velocity $U = VR_0/L$ is chosen to be equal to the shear velocity at a distance R_0 from the center. The characteristic viscosity η_0 is chosen as the viscosity of the fluid at the exterior of the membrane.

The following four dimensionless numbers are introduced:

$$Re = \frac{\rho R_0 U}{\eta_0}, \quad Ca = \frac{\eta_0 R_0^2 U}{k}, \quad \alpha = \frac{R_0}{L} \quad \text{and} \quad \beta = \frac{\eta_1}{\eta_0}$$

The Reynolds number Re, as usual, expresses the ratio of inertia effects to the viscous ones. The capillarity number Ca compares the strength of the imposed flow $\eta_0 U/R_0$ to the bending resistance of the membrane k/R_0^3. The dimensionless number α represents the confinement of the vesicle in the shear flow and β is the viscosity ratio. The initial shape $\partial\Omega(0)$ is also characterized by a fifth dimensionless number: γ, the reduced area, already introduced in (2).

In the rest of the paper, only dimensionless quantities are used and, since there is no ambiguity, there are still denoted with the same notations as the original quantities. The dimensionless version of the boundary condition writes:

$$\mathbf{u}_b(t, x) = \begin{cases} 1/\alpha & \text{when } x_d = \alpha \\ -1/\alpha & \text{when } x_d = -\alpha \end{cases}$$

A dimensionless viscosity function is also defined:

$$\eta_*(t, x) = \begin{cases} \beta & \text{when } x \in \Omega(t) \\ 1 & \text{otherwise} \end{cases}$$

The dimensionless problem writes:

find ϕ, $\mathbf{u}$, p *and* λ *such that*

$$\frac{\partial \phi}{\partial t} + \mathbf{u}.\nabla\phi = 0 \text{ in }]0,T[\times\Lambda \quad (7a)$$

$$Re\left(\frac{\partial \mathbf{u}}{\partial t} + \mathbf{u}.\nabla\mathbf{u}\right) - \mathbf{div}\left(2\eta_* D(\mathbf{u})\right) + \nabla p = 0 \text{ in }]0,T[\times(\Lambda\backslash\partial\Omega) \quad (7b)$$

$$\operatorname{div}\mathbf{u} = 0 \text{ in }]0,T[\times\Lambda \quad (7c)$$

$$\operatorname{div}_s \mathbf{u} = 0 \text{ on }]0,T[\times\partial\Omega \quad (7d)$$

$$[\mathbf{u}] = 0 \text{ on }]0,T[\times\partial\Omega \quad (7e)$$

$$-\frac{1}{Ca}\left\{\Delta_s H + H\left(\frac{H^2}{2} - 2K\right)\right\}\mathbf{n} + H\,\lambda\,\mathbf{n} - \nabla_s\lambda + \left[2\eta_* D(\mathbf{u}) - pI\right].\mathbf{n} = 0 \text{ on }]0,T[\times\partial\Omega \quad (7f)$$

$$\phi = \phi_b \text{ on }]0,T[\times\Sigma_- \quad (7g)$$

$$\mathbf{u} = \mathbf{u}_b \text{ on }]0,T[\times\Sigma_D \quad (7h)$$

$$(2\eta^* D(\mathbf{u}) - pI).\boldsymbol{\nu} = 0 \text{ on }]0,T[\times\Sigma_N \quad (7i)$$

$$\phi(0) = \phi_0 \text{ in } \Lambda \quad (7j)$$

$$\mathbf{u}(0) = \mathbf{u}_0 \text{ in } \Lambda \quad (7k)$$

where the normal and the curvature are expressed in term of the level set function: $\mathbf{n} = \nabla\phi/|\nabla\phi|$ and $H = \operatorname{div}_s \mathbf{n}$. Biophysical applications, as the prediction of vesicles behavior in small blood vessels, is our aim in this paper, and constitute a guideline for the choice of dimensionless parameters. Following Vitkova and al. [52] on vesicles under shear flow, we estimate the physical parameters:

$$\begin{array}{lllllll} R_0 & \approx & 5\times10^{-5} & \text{m}, & \rho & \approx & 10^3 \quad \text{kg/m}^3, \\ L & \approx & 10^{-3} & \text{m}, & \eta_0 & \in & [5\times10^{-4},\ 0.2] \quad kg.s^{-1}.m^{-1}, \\ k & \approx & 10^{-19} & \text{J}. & & & \end{array}$$

The shear velocity at the wall V is between 1.2×10^{-2} and 0.12 m/s. These experimental values leads to consider the following dimensionless parameter ranges:

$$\begin{aligned} Re &\in \left[1.5\times10^{-9},\ 1.5\times10^{-4}\right], \\ Ca &\in \left[3\times10^{3},\ 3\times10^{6}\right]. \end{aligned}$$

The vesicles are deflated with γ between 0.92 and 0.99. While the experimental value of the confinement was $\alpha = 1/20$, the influence of this parameter is studied by varying its value between 1/2 and 1/5 in the case of regular meshes and reaching 1/12 when using adaptive meshes methods, as presented in the next section. Finally, the viscosity ratio β is varying around a critical value associated to a stability transition and is taken less than 20.

2.4 Variational formulation

Let us introduce the following space of admissible velocities:

$$\mathbb{V}(\mathbf{u}_b) \;=\; \left\{\mathbf{v}\in\left(H^1(\Lambda)\right)^d;\ \mathbf{v}=\mathbf{u}_b \ \text{ on } \Sigma_D\right\}.$$

Equation (7b) is multiplied by a test function $\mathbf{v}\in\mathbb{V}(0)$ and then integrated by parts on Ω and $\Lambda\backslash\overline{\Omega}$ separately. Then, terms are then merged and we get:

$$\int_\Lambda Re\,\frac{D\mathbf{u}}{Dt}.\mathbf{v}\,\mathrm{d}x-\int_\Lambda \mathbf{div}\left(2\eta^*\,D(\mathbf{u})-pI\right).\mathbf{v}\,\mathrm{d}x+\int_{\partial\Lambda}\left\{\left(2\eta^*\,D(\mathbf{u})-pI\right).\boldsymbol{\nu}\right\}.\mathbf{v}\,\mathrm{d}s$$
$$+\int_{\partial\Omega(t)}\left\{\left[2\eta^*\,D(\mathbf{u})-pI\right].\mathbf{n}\right\}.\mathbf{v}\,\mathrm{d}s-\int_{\partial\Omega(t)}\nabla_s\lambda.\mathbf{v}\,\mathrm{d}s+\int_{\partial\Omega(t)}\lambda\,H\mathbf{n}.\mathbf{v}\;\mathrm{d}s$$
$$=\int_{\partial\Omega(t)}\mathbf{f}.\mathbf{v}\,\mathrm{d}s$$

where I is the identity tensor and **div** is the divergence of a symmetric tensor, defined as the divergence of its row or column vectors. We have introduced the material time derivative $\dfrac{D\mathbf{u}}{Dt}=\partial_t\mathbf{u}+\mathbf{u}.\nabla\mathbf{u}$. The strength $\mathbf{f}$, that appears in the right-hand-side of the previous relation is associated to the Canham-Helfrich bending energy:

$$\mathbf{f}=\frac{1}{Ca}\left\{\Delta_s H+H\left(\frac{H^2}{2}-2K\right)\right\}\mathbf{n}.$$

In the two-dimensional case, since $K=0$, this expression reduces to: $\mathbf{f}=Ca^{-1}\left(\Delta_s H+H^3/2\right)\mathbf{n}$. In order for the integral term involving $\mathbf{f}$ to be well defined, we suppose that the interface $\partial\Omega(t)$ is sufficiently regular, e.g. C^4.

In order to deal with the integrals over $\partial\Omega(t)$, a generalization of the Green formula over the closed surface $\partial\Omega(t)$ is used (see e.g. [35]):

$$\int_{\partial\Omega}\nabla_s\mu.\mathbf{v}\,\mathrm{d}s+\int_{\partial\Omega}\mu\,\mathrm{div}_s\,\mathbf{v}\,\mathrm{d}s=\int_{\partial\Omega}\mu\,\mathbf{v}.\mathbf{n}\,H\,\mathrm{d}s,\quad\forall\mu\in H^{\frac{1}{2}}(\partial\Omega),\quad\forall\mathbf{v}\in H^1(\Lambda). \tag{8}$$

The previous equations leads to the following variational formulation of the problem: *find* $\mathbf{u}\in C^0\left(]0,T[,L^2(\Lambda)^d\right)\cap L^2\left(]0,T[,\mathbb{V}(\mathbf{u}_b)\right)$, $p\in L^2\left(]0,T[,L^2_0(\Omega)\right)$ *and* $\lambda\in L^2\left(]0,T[,H^{\frac{1}{2}}(\partial\Omega)\right)$ *such that*

$$\int_\Lambda Re\,\frac{D\mathbf{u}}{Dt}.\mathbf{v}\,\mathrm{d}x+\int_\Lambda 2\eta^*\,D(\mathbf{u}):D(\mathbf{v})\,\mathrm{d}x$$
$$+\int_\Lambda p\;\mathrm{div}\,\mathbf{v}\,\mathrm{d}x+\int_{\partial\Omega(t)}\lambda\,\mathrm{div}_s\,\mathbf{v}\,\mathrm{d}s \;=\; \int_{\partial\Omega(t)}\mathbf{f}.\mathbf{v}\,\mathrm{d}s,\quad\forall\mathbf{v}\in\mathbb{V}(0), \tag{9a}$$
$$\int_\Lambda q\;\mathrm{div}\,\mathbf{u}\,\mathrm{d}x \;=\; 0,\quad\forall q\in L^2(\Lambda), \tag{9b}$$
$$\int_{\partial\Omega(t)}\mu\,\mathrm{div}_s\,.\mathbf{u}\,\mathrm{d}s \;=\; 0,\quad\forall\mu\in H^{\frac{1}{2}}(\partial\Omega(t)). \tag{9c}$$

together with the initial condition $\mathbf{u}(0) = \mathbf{u}_0$. Recall that $\partial\Omega(t)$ is given by (3) in terms of the level set function ϕ, which is solution of the transport problem (4a)-(4c) involving $\mathbf{u}$.

2.5 Remarks on the Lagrange multipliers

The stationnary problem can be expressed as a minimization one: this formulation is useful in order to understand the structure of the set of equations and the relations between the velocity field $\mathbf{u}$ and the two Lagrange multipliers p and λ. Let us introduce the following space of admissible velocities:

$$\mathbb{K}(\mathbf{u}_b) \quad = \quad \{\mathbf{v} \in \mathbb{V}(\mathbf{u}_b);\ \operatorname{div}\mathbf{v} = 0 \text{ in } \Lambda \text{ and } \operatorname{div}_s \mathbf{v} = 0 \text{ on } \partial\Omega\}\,.$$

For any shape Ω and any admissible velocity field $\mathbf{u}$ defined in Λ, the energy of the system is defined by:

$$J(\mathbf{u}) = \int_\Lambda \eta^* \left| D\left(\mathbf{u}\right)\right|^2 \mathrm{d}x + \frac{1}{2Ca}\int_{\partial\Omega} H^2\,\mathrm{d}s, \tag{10}$$

where $|.|$ denotes the Euclidean norms of vectors or tensors. The previous expression of the energy includes two terms: the viscous energy involving $\mathbf{u}$ and the Canham-Helfrich bending energy, involving the shape Ω of the vesicle. Notice that, in the bending energy term in (10), the membrane $\partial\Omega$ depends upon the velocity field $\mathbf{u}$ via (3) and the level-set function ϕ, satisfying the transport problem (4) that involves $\mathbf{u}$. Also, the curvature H on $\partial\Omega$ depends implicitly upon $\mathbf{u}$. Remark that J is not convex in general: the optimality system $J'(\mathbf{u}) = 0$ could include both minimums and maximums of the energy J. Thus, this optimality system is not equivalent to the minimization of the energy. Nevertheless, a minimum of J is also a solution of the optimality system.

The problem expresses as a minimization one:

$$\mathbf{u} = \underset{\mathbf{v}\in\mathbb{K}(t,\mathbf{u}_b)}{\arg\inf}\, J(\mathbf{v}).$$

where $\mathbf{u}_0$ is the given initial velocity. This is a strongly nonlinear shape optimization problem, expressed in terms of the unknown $\mathbf{u}$.

The space of admissible velocities $\mathbb{K}(t, \mathbf{u}_b)$ contains the incompressibility and inextensibility constraints: it is not suitable for practical finite element discretization, since there are no known finite element basis of such spaces. Conversely, the unconstrained space of $\mathbb{V}(\mathbf{u}_b)$ is of practical interest: the two constraints can be imposed via two Lagrange multipliers: the pressure p and the surface tension λ. Let us introduce the following Lagrangian:

$$\mathscr{L}(\mathbf{u};\, p, \lambda) = J(\mathbf{u}) + \int_\Lambda p \operatorname{div}\mathbf{u}\,\mathrm{d}x + \int_{\partial\Omega} \lambda \operatorname{div}_s \mathbf{v}\,\mathrm{d}s.$$

The previous minimization problem can be rewritten as a saddle point problem:

$$(\mathbf{u}, p, \lambda) = \underset{\mathbf{v}\in\mathbb{V}(\mathbf{u}_b)}{\arg\inf} \sup_{\substack{q\in L^2(\Lambda)\\ \mu\in H^{\frac{1}{2}}(\partial\Omega)}} \mathscr{L}(\mathbf{v};\, q, \mu).$$

Here $H^{\frac{1}{2}}(\partial\Omega)$ denotes as usual [1] the space of the trace of elements of $H^1(\Omega)$ on $\partial\Omega$. Thus, p and λ are two Lagrange multipliers, associated respectively to the local mass and area conservations constraints. The minimization and saddle-points principles do not extend to the time-dependent case, due to the presence of the inertia term.

3 Numerical methods

3.1 Time discretization and the characteristic method

For simplicity, the numerical methods are presented when $d = 2$: in that case the Gauss curvature is null: $K = 0$. Nevertheless, the methods extend to three-dimensional case, just inserting the computation of K in the Canham-Helfrich force.

Let $0 = t^0 < t^1 < t^2 < ... < t^N = T$ be a subdivision of the time interval $[0, T]$ with a constant time step $\Delta t = t^{n+1} - t^n$, $n = 1, 2, ..., N$. At step $n = 0$, let $\phi^0 = \phi_0$ be the initial condition. For any $n \geq 1$, the unknowns ϕ^n, $\mathbf{u}^n$, p^n and λ^n at time step n are computed by induction, using values at previous time steps. The time discretization is performed by using the method of characteristics: for any $t > 0$ and $x \in \Lambda$, the characteristic curve $X(., x, ; t)$ passing at time t through x is defined by the following ordinary differential equation:

$$\left\{ \begin{array}{rcl} \dfrac{\partial X}{\partial t}(s, x; t) & = & \mathbf{u}\left(X(s, x; t), t\right), \quad s \in]0, T[\\ X(t, x; t) & = & x. \end{array} \right.$$

For any function $\varphi(t, x)$, the total derivative $D\varphi/Dt$ expresses:

$$\frac{D\varphi}{Dt}(t, x) = \left(\frac{\partial \varphi}{\partial t} + \mathbf{u}.\nabla\varphi\right)(t, x) = \frac{\partial}{\partial \tau}\left(\varphi\left(X(t, x; \tau), \tau\right)\right)|_{\tau=t}$$

Following Pironneau [43], this derivative is approximated by a first-order backward Euler scheme:

$$\frac{D\varphi}{Dt}(t^n, x) \approx \frac{\varphi(t^n, x) - \varphi(t^{n-1}, X_1^{n-1}(x))}{\Delta t}$$

where $X_1^{n-1}(x) = x - \Delta t\ \mathbf{u}^{n-1}(x)$ denotes the first-order forward Euler approximation of $X(t^{n-1}, x; t^n)$. The time-discretization of the transport equation (7a) leads to:

$$\phi^n = \phi^{n-1} \circ X_1^{n-1} \quad \text{in } \Lambda \tag{11}$$

Then, the vesicle shape at step n is known:

$$\begin{aligned} \partial\Omega^n &= \{x \in \Lambda;\ \phi^n(x) = 0\} \\ \Omega^n &= \{x \in \Lambda;\ \phi^n(x) < 0\} \end{aligned}$$

The dimensionless viscosity is also computed explicitly:

$$\eta_*^n = \begin{cases} \beta & \text{when } x \in \Omega^n \\ 1 & \text{otherwise} \end{cases}$$

Also, the normal $\mathbf{n}^n$ and the curvature H^n are computed at this step, together with differential operators (5) on the surface $\partial\Omega^n$, and defined for any scalar function f and any vector field $\mathbf{v}$ by:

$$\nabla_s^n f = (I - \mathbf{n}^n \otimes \mathbf{n}^n)\ \nabla f, \tag{12a}$$

$$\mathrm{div}_s^n\, \mathbf{v} = (I - \mathbf{n}^n \otimes \mathbf{n}^n) : \nabla \mathbf{v}, \tag{12b}$$

$$\Delta_s^n f = \mathrm{div}_s^n\ (\nabla_s^n f)\,. \tag{12c}$$

For any $y \in \mathcal{C}^3([0,T])$, a Taylor expansion shows that:

$$\frac{\mathrm{d}y}{\mathrm{d}t}(t) = \frac{3y(t) - 4y(t-\Delta t) + y(t-2\Delta t)}{2\Delta t} + \mathcal{O}\left(\Delta t^2\right).$$

Based on this approximation and following [49, chap. 5], the time discretization of the inertia term is performed by using a second order combined characteristic and finite difference discretization method. Let us introduce the second-order characteristics:

$$\begin{aligned} \mathbf{u}^* &= 2\mathbf{u}^{n-1} - \mathbf{u}^{n-2} \\ X_2^{n-1}(x) &= x - \Delta t\ \mathbf{u}^*(x) \quad \text{a.e. } x \in \Lambda, \\ X_2^{n-2}(x) &= x - 2\Delta t\ \mathbf{u}^*(x) \quad \text{a.e. } x \in \Lambda. \end{aligned}$$

Notice that $\mathbf{u}^*$ represents a prediction by extrapolation of $\mathbf{u}$ at time t_n. The problem becomes:

find $\mathbf{u}^n$, p^n *and* λ^n *such that*

$$\frac{Re}{2\Delta t}\left(3\mathbf{u}^n - 4\mathbf{u}^{n-1}oX_2^{n-1} + \mathbf{u}^{n-2}oX_2^{n-2}\right)$$

$$-\mathbf{div}\left(2\eta_*^n D\left(\mathbf{u}^n\right)\right) + \nabla p^n = 0 \quad \text{in } \Lambda\backslash\partial\Omega^n, \tag{13a}$$

$$\operatorname{div}\mathbf{u}^n = 0 \quad \text{in } \Lambda, \tag{13b}$$

$$\left[\mathbf{u}^n\right] = 0 \quad \text{on } \partial\Omega^n, \tag{13c}$$

$$-\frac{1}{Ca}\left(\Delta_s^n H^n + \frac{\left(H^n\right)^3}{2}\right)\mathbf{n}^n + H^n\lambda^n\mathbf{n}^n - \nabla_s^n\lambda^n$$

$$+\left[2\eta_*^n D\left(\mathbf{u}^n\right) - p^n\mathbf{I}\right].\mathbf{n}^n = 0 \quad \text{on } \partial\Omega^n, \tag{13d}$$

$$\operatorname{div}_s^n.\mathbf{u}^n = 0 \quad \text{on } \partial\Omega^n, \tag{13e}$$

$$\mathbf{u}^n = \mathbf{u}_b \quad \text{on } \Sigma_D. \tag{13f}$$

The second order induction on $\left(\mathbf{u}^n\right)_{n\geq 0}$ is bootstrapped by using the initial condition: $\mathbf{u}^{-1} = \mathbf{u}^0 = \mathbf{u}_0$, where $\mathbf{u}^{-1}$ stands here for a convenient notation. The previous scheme uses two main steps. The first step (11) is an explicit computation involving the characteristics. The second step (13) is a linear generalized Stokes sub-system that involves a constraint on the boundary of the vesicle together with the usual incompressibility constraint. We point out that this scheme transforms a strongly nonlinear shape optimization problem into a succession of explicit computations and linear subproblems. The next paragraph presents how such a linear subproblem is treated.

3.2 The generalized Stokes subproblem

3.2.1 Formulation

Let us introduce the Canham-Helfrich force, that appears in the right-hand side of the generalized Stokes subproblem:

$$\mathbf{f}^n = \frac{1}{Ca}\left(\Delta_s^n H^n + \frac{\left(H^n\right)^3}{2}\right)\mathbf{n}^n. \tag{14}$$

where $\mathbf{n}^n = \nabla\phi^n/|\nabla\phi^n|$, $H^n = \mathrm{div}_s\,\mathbf{n}^n$ and ϕ^n is known at this step of the algorithm. The following bilinear forms are first introduced:

$$\begin{aligned}
m(\mathbf{u},\mathbf{v}) &= \int_\Lambda \mathbf{u}.\mathbf{v}\,\mathrm{d}x,\ \forall \mathbf{u},\mathbf{v} \in \left(L^2(\Lambda)\right)^2,\\
a^n(\mathbf{u},\mathbf{v}) &= \int_\Lambda 2\,\eta_*^n\, D(\mathbf{u}) : D(\mathbf{v})\,\mathrm{d}x,\ \forall \mathbf{u},\mathbf{v} \in \left(H^1(\Lambda)\right)^2,\\
b_1(\mathbf{v},q) &= -\int_\Lambda q\,\mathrm{div}\,\mathbf{v}\,\mathrm{d}x,\ \forall q \in L^2(\Lambda),\ \forall \mathbf{v} \in H(\mathrm{div},\Lambda),\\
b_2^n(\mathbf{v},\mu) &= -\int_{\partial\Omega^n} \mu\,\mathrm{div}_s^n\,\mathbf{v}\,\mathrm{d}s,\ \forall \mu \in H^{\frac{1}{2}}(\partial\Omega^n),\ \forall \mathbf{v} \in H(\mathrm{div}_s,\partial\Omega^n).
\end{aligned}$$

where $H(\mathrm{div},\Lambda) = \left\{\mathbf{s} \in \left(L^2(\Lambda)\right)^2;\ \mathrm{div}\,\mathbf{s} \in L^2(\Lambda)\right\}$ (see e.g. [22, 11]). The variational formulation of (13a)-(13f) writes:

(S): *find* $\mathbf{u}^n \in \mathbb{V}(\mathbf{u}_b)$, $p^n \in L^2(\Lambda)$ *and* $\lambda^n \in H^{\frac{1}{2}}(\partial\Omega^n)$ *such that*

$$\begin{aligned}
&\frac{3Re}{2\Delta t} m\left(\mathbf{u}^n,\mathbf{v}\right) + a^n\left(\mathbf{u}^n,\mathbf{v}\right) + b_1\left(\mathbf{v},p^n\right) + b_2^n\left(\mathbf{v},\lambda^n\right)\\
&= m_s^n\left(\mathbf{f}^n,\mathbf{v}\right) + \frac{Re}{2\,\Delta t} m\left(4\mathbf{u}^{n-1}oX_2^{n-1} - \mathbf{u}^{n-2}oX_2^{n-2},\mathbf{v}\right), \qquad (15a)\\
&b_1\left(\mathbf{u}^n,q\right) = 0, \qquad (15b)\\
&b_2^n\left(\mathbf{u}^n,\mu\right) = 0, \qquad (15c)
\end{aligned}$$

for all $\mathbf{v} \in \mathbb{V}(0)$, $q \in L^2(\Lambda)$ and $\mu \in H^{\frac{1}{2}}(\partial\Omega^n)$.

3.2.2 The Canham-Helfrich force

Let us consider in details the Canham-Helfrich force, as defined in (14). The force involves fourth order derivatives of the level set function and a direct discretization approach would requires a high regularity finite element method, such as the Hermite one (see e.g. [10]) with H^2 and C^1 regularity. In order to use standard Lagrange finite element, with only H^1 and C^0 regularity, the fourth-order derivatives are treated here with a different approach, based on a duality argument.

Since $H^n = \mathrm{div}\,\mathbf{n}^n$ and $\mathbf{n}^n = \nabla\phi^n/|\nabla\phi^n|$, then H^n involves the second order derivative of the level set function. Let us define the *skeleton* of Ω as the set of points that are equidistant to at least two distinct points of $\partial\Omega$ (see e.g. [3, p. 195]). In order to avoid division by $|\nabla\phi^n|$, that could vanish on the skeleton, two intermediate variables $\mathbf{r}^n = \nabla(|\nabla\phi^n|)$ and $G^n = H^n|\nabla\phi^n|$ are used. First, using a classical Green formula in Λ, $\mathbf{r}^n$ can be characterized as

$$\mathbf{r}^n \in H_0(\mathrm{div},\Lambda) \text{ and } \int_\Lambda \mathbf{r}^n.\mathbf{s}\,\mathrm{d}x = \int_\Lambda |\nabla\phi^n|\ \mathrm{div}\,\mathbf{s}\ \mathrm{d}x, \quad \forall \mathbf{s} \in H_0(\mathrm{div},\Lambda),$$

where $H_0(\mathrm{div},\Lambda)=\{\mathbf{s}\in H(\mathrm{div},\Lambda);\ \mathbf{s}.\boldsymbol{\nu}=0\}$. Next, let us turn to G^n. A simple development leads to:

$$G^n|\nabla\phi^n| = -H^n\ |\nabla\phi^n|^2 = -\mathrm{div}\left(\frac{\nabla\phi^n}{|\nabla\phi^n|}\right)|\nabla\phi^n|^2 = \mathbf{r}^n.\nabla\phi^n - \Delta\phi^n|\nabla\phi^n|$$

The duality argument is used for the $\Delta\phi^n$ term at the right-hand side and G^n is characterized by

$$G^n\in H^1(\Lambda)\ \text{ and }\ \int_\Lambda G^n\,\zeta\,|\nabla\phi^n|\,\mathrm{d}x = \int_\Lambda(\mathbf{r}^n.\nabla\phi^n)\,\zeta\,\mathrm{d}x + \int_\Lambda\nabla\phi^n.\nabla\zeta\,|\nabla\phi^n|\,\mathrm{d}x,\ \forall\zeta\in H^1(\Lambda).$$

Finally, H^n is defined as the restriction to $\partial\Omega^n$ of $G^n/|\nabla\phi^n|$. Notice that this quantity is well defined since $|\nabla\phi^n|$ is not vanishing at the vicinity of $\partial\Omega^n$.

Let us consider the following Green formula on the closed surface $\Gamma^n=\partial\Omega^n$:

$$\int_{\Gamma^n}\Delta_s^n\xi\,\zeta\,\mathrm{d}s + \int_{\Gamma^n}\nabla_s^n\xi.\nabla_s^n\zeta\,\mathrm{d}s = 0,\ \forall\xi,\zeta\in H^1(\Gamma^n).$$

Then $Y^n=-\Delta_s H^n$ can be computed in a weak sense:

$$Y^n\in H^1(\partial\Omega^n)\ \text{ and }\ \int_{\partial\Omega^n}Y^n\,\zeta\,\mathrm{d}s = \int_{\partial\Omega^n}\nabla_s^n H^n.\nabla_s^n\zeta\,\mathrm{d}s,\ \forall\zeta\in H^1(\partial\Omega^n)$$

Let us summarize the procedure. The following additional bilinear forms are introduced:

$$\begin{aligned}
m_w^n(\phi,\psi) &= \int_\Lambda\varphi\,\psi\,|\nabla\phi^n|\,\mathrm{d}x,\ \forall\varphi,\psi\in L^2(\Lambda),\\
a_w^n(\phi,\psi) &= \int_\Lambda\nabla\varphi\,\nabla\psi\,|\nabla\phi^n|\,\mathrm{d}x,\ \forall\varphi,\psi\in H^1(\Lambda),\\
m_s^n(\xi,\zeta) &= \int_{\partial\Omega^n}\xi\,\zeta\,\mathrm{d}s,\ \forall\xi,\zeta\in L^2(\partial\Omega^n),\\
c^n(\xi,\zeta) &= \int_{\partial\Omega^n}\nabla_s^n\xi.\nabla_s^n\zeta\,\mathrm{d}s,\ \forall\xi,\zeta\in H^1(\partial\Omega^n).
\end{aligned}$$

Then, compute successively as:

$$\begin{aligned}
\mathbf{r}^n\in H_0(\mathrm{div},\Lambda)\text{ and }m(\mathbf{r}^n,\mathrm{s}) &= -b_1(|\nabla\phi^n|,\,\mathbf{s}^n),\ \forall\mathbf{s}\in H_0(\mathrm{div},\Lambda),\\
G^n\in H^1(\Lambda)\text{ and }m_w^n(G^n,\psi) &= a_w^n(\phi^n,\psi)+m(\mathbf{r}^n.\nabla\phi^n,\psi),\ \forall\psi\in H^1(\Lambda),\\
H^n &= \frac{G^n}{|\nabla\phi^n|}\ \text{ on }\ \partial\Omega^n,\\
Y^n\in H^1(\partial\Omega^n)\text{ and }m_s^n(Y^n,\zeta) &= c^n(H^n,\zeta),\ \forall\zeta\in H^1(\partial\Omega^n),\\
\mathbf{n}^n &= \frac{\nabla\phi^n}{|\nabla\phi^n|}\ \text{ on }\ \partial\Omega^n,\\
\mathbf{f}^n &= \frac{1}{Ca}\left(-Y^n+\frac{(H^n)^3}{2}\right)\mathbf{n}^n\ \text{ on }\ \partial\Omega^n.
\end{aligned}$$

3.2.3 Extension and regularization

The previous variational formulation involves integrals over the moving surface $\partial\Omega^n$: in order to avoid the explicit re-triangulation of the surface $\partial\Omega^n$ at each time step, integrals over $\partial\Omega^n$ are transformed into integrals over Λ. First, remarks that an integral over $\partial\Omega^n$ can be written as an integral over Λ with the help of the level set function ϕ^n and the Dirac measure δ:

$$\int_{\partial\Omega^n} \varphi \, \mathrm{d}s = \int_{\Lambda} \tilde{\varphi} \, |\nabla\phi^n| \, \delta(\phi^n) \, \mathrm{d}x$$

where $\tilde{\varphi}$ is an extension to Λ of any function φ defined in $\partial\Omega^n$. Also, the normal vector $\mathbf{n}^n$, defined over $\partial\Omega^n$, extends as $\nabla\phi^n/|\nabla\phi^n|$ to Λ. Since there is no ambiguity, this extension of the normal is still denoted by $\mathbf{n}^n$. Also, the notations for the extension to Λ of the surface operators defined in (12) are still conserved. By this way, the Canham-Helfrich force, as expressed by (14), can be extended to Λ.

Nevertheless, the explicit management of Dirac measures is not an easy task in finite element methods. Thus, the previous extension is combined together with a regularization procedure. Three sharp functions are here considered: the Heaviside function $\mathscr{H}(\phi^n)$, that acts as the indicator of $\Lambda\backslash\Omega^n$, the Dirac measure $\delta(\phi^n)$ that localizes the surface $\partial\Omega^n$, and the sign function $\mathrm{sgn}(\phi^n)$, that will be used in a forthcoming paragraph, for redistancing the level set function.

In order to avoid the triangulation of $\partial\Omega^n$, a banded region of width 2ε is introduced, for some $\varepsilon > 0$. The Heaviside $\mathscr{H}$, the Dirac δ and the sign functions are replaced respectively by $\mathscr{H}_\varepsilon$, δ_ε and sgn_ε, defined for all $\phi \in \mathbb{R}$ by:

$$\begin{aligned}
\mathscr{H}_\varepsilon(\phi) &= \begin{cases} 0, & \text{when } \phi < -\varepsilon, \\ \dfrac{1}{2}\left(1 + \dfrac{\phi}{\varepsilon} + \dfrac{\sin\left(\dfrac{\pi\phi}{\varepsilon}\right)}{\pi}\right), & \text{when } |\phi| \le \varepsilon, \\ 1, & \text{otherwise,} \end{cases} \\
\delta_\varepsilon(\phi) &= \frac{\mathrm{d}\mathscr{H}_\varepsilon}{\mathrm{d}\phi}(\phi) = \begin{cases} \dfrac{1}{2\varepsilon}\left(1 + \cos\left(\dfrac{\pi\phi}{\varepsilon}\right)\right), & \text{if } |\phi| \le \varepsilon \\ 0, & \text{otherwise} \end{cases} \\
\mathrm{sgn}_\varepsilon(\phi) &= 2\mathscr{H}_\varepsilon(\phi) - 1
\end{aligned}$$

The sharp viscosity is also replaced by a smooth one:

$$\eta^n_{*,\varepsilon} = \beta + (1-\beta)\mathscr{H}_\varepsilon\left(\phi^n\right)$$

The previous bilinear forms admits a regularized counterpart:

$$\begin{aligned}
a_\varepsilon^n(\mathbf{u},\mathbf{v}) &= \int_\Lambda 2\,\eta_{*,\varepsilon}^n\, D(\mathbf{u}) : D(\mathbf{v})\,\mathrm{d}x,\ \forall \mathbf{u},\mathbf{v} \in \left(H^1(\Lambda)\right)^2,\\
m_{s,\varepsilon}^n(\mathbf{u},\mathbf{v}) &= \int_\Lambda \mathbf{u}.\mathbf{v}\,|\nabla\phi^n|\,\delta_\varepsilon\left(\phi^n\right)\,\mathrm{d}x,\ \forall \mathbf{u},\mathbf{v} \in \left(L^2(\Lambda)\right)^2,\\
b_{2,\varepsilon}^n(\mathbf{v},\mu) &= -\int_\Lambda \mu\,\mathrm{div}_s^n\,\mathbf{v}\,|\nabla\phi^n|\,\delta_\varepsilon\left(\phi^n\right)\,\mathrm{d}x,\ \forall \mu \in L^2(\Lambda),\ \forall \mathbf{v} \in \left(H^1(\Lambda)\right)^2,\\
c_\varepsilon^n(\xi,\zeta) &= \int_\Lambda \nabla_s^n\xi.\nabla_s^n\zeta\,|\nabla\phi^n|\,\delta_\varepsilon\left(\phi^n\right)\,\mathrm{d}x,\ \forall \xi,\zeta \in H^1(\Lambda)
\end{aligned}$$

The computation of the curvature H^n is unchanged while the Canham-Helfrich force becomes: find $Y_\varepsilon^n \in H^1(\Lambda)$ such that

$$m_{s,\varepsilon}(Y_\varepsilon^n,\zeta) = c_\varepsilon(H^n,\zeta),\ \forall \zeta \in H^1(\Lambda).$$

Then, compute the extension to Λ of the force:

$$\mathbf{f}_\varepsilon^n = \frac{1}{Ca}\left(-Y_\varepsilon^n + \frac{\left(H^n\right)^3}{2}\right)\mathbf{n}^n \ \text{ in } \Lambda.$$

Problem (15) admits a regularized variant:

$(S)_\varepsilon$: *find* $\mathbf{u}_\varepsilon^n \in \mathbb{V}(\mathbf{u}_b)$, $p_\varepsilon^n \in L^2(\Lambda)$ *and* $\lambda_\varepsilon^n \in L^2(\Lambda)$ *such that*

$$\begin{aligned}
&\frac{3Re}{2\Delta t} m\left(\mathbf{u}_\varepsilon^n,\mathbf{v}\right) + a_\varepsilon^n\left(\mathbf{u}_\varepsilon^n,\mathbf{v}\right) + b_1\left(\mathbf{v},p_\varepsilon^n\right) + b_{2,\varepsilon}^n\left(\mathbf{v},\lambda_\varepsilon^n\right)\\
&= m_{s,\varepsilon}^n\left(\mathbf{f}_\varepsilon^n,\mathbf{v}\right) + \frac{Re}{2\,\Delta t} m\left(4\mathbf{u}_\varepsilon^n oX_2^n - \mathbf{u}_\varepsilon^{n-1} oX_2^{n-1},\mathbf{v}\right), \qquad (16a)\\
&b_1\left(\mathbf{u}_\varepsilon^n,q\right) = 0, \qquad (16b)\\
&b_{2,\varepsilon}^n\left(\mathbf{u}_\varepsilon^n,\mu\right) = 0, \qquad (16c)
\end{aligned}$$

for all $\mathbf{v} \in \mathbb{V}(0)$, $q \in L^2(\Lambda)$ and $\mu \in L^2(\Lambda)$. Notice that the surface tension λ_ε^n is now extended to Λ. The regularization parameter ε will be chosen as proportional to the the mesh size h, as presented in the next paragraph.

3.2.4 Finite element discretization

The Taylor-Hood finite element approximation (see e.g. [11]) for the Stokes problem is considered here for the velocity-pressure approximation of the generalized Stokes problem. Let $\mathscr{T}_h$ a finite element triangulation of Λ, where $h > 0$ stands for the largest element diameter [10]. The following finite dimensional spaces are

introduced:

$$\begin{aligned} X_h &= \left\{ q \in C^0\left(\overline{\Lambda}\right),\ q_{|K} \in \mathbb{P}_1,\ \forall K \in \mathscr{T}_h \right\}, \\ \mathbf{S}_h &= \left\{ \mathbf{s} \in X_h^2,\ \mathbf{s}.\boldsymbol{\nu} = 0 \text{ on } \partial\Lambda \right\}, \\ \mathbb{X}_h &= \left\{ \mathbf{u} \in \left(C^0\left(\overline{\Lambda}\right)\right)^2,\ \mathbf{u}_{|K} \in \left(\mathbb{P}_2\right)^d,\ \forall K \in \mathscr{T}_h \right\}, \\ \mathbb{V}_h(\mathbf{u}_b) &= \mathbb{X}_h \cap \mathbb{V}(\mathbf{u}_b). \end{aligned}$$

Let us assume that $\phi_h^n \in X_h$ is an approximation of ϕ^n at the n-th time step. The computation of the discrete Canham-Helfrich force write:

$$\begin{aligned} \mathbf{r}_h^n \in S_h \text{ and } m(\mathbf{r}_h^n, \mathrm{s}) &= -b_1(|\nabla\phi_h^n|, \mathbf{s}^n),\ \forall \mathbf{s} \in S_h, \\ G_h^n \in X_h \text{ and } m_w^n(G_h^n, \psi) &= a_w^n(\phi_h^n, \psi) + m(\mathbf{r}_h^n.\nabla\phi_h^n, \psi),\ \forall \psi \in X_h, \\ H_h^n &= \frac{G_h^n}{|\nabla\phi_h^n|} \text{ in } \Lambda, \\ Y_h^n \in X_h \text{ and } m_{s,\varepsilon}(Y_h^n, \zeta) &= c_\varepsilon(H_h^n, \zeta),\ \forall \zeta \in X_h, \\ \mathbf{n}_h^n &= \frac{\nabla\phi_h^n}{|\nabla\phi_h^n|} \text{ in } \Lambda, \\ \mathbf{f}_h^n &= \frac{1}{Ca}\left(-Y_h^n + \frac{\left(H_h^n\right)^3}{2}\right)\mathbf{n}_h^n \text{ in } \Lambda. \end{aligned}$$

The discrete generalized Stokes problem writes:

$(S)_h$: *find* $\mathbf{u}_h^n \in \mathbb{V}_h(\mathbf{u}_b)$, $p_h^n \in X_h$ *and* $\lambda_h^n \in X_h$ *such that*

$$\begin{aligned} &\frac{3Re}{2\Delta t} m\left(\mathbf{u}_h^n, \mathbf{v}\right) + a_\varepsilon^n\left(\mathbf{u}_h^n, \mathbf{v}\right) + b_1\left(\mathbf{v}, p_h^n\right) + b_{2,\varepsilon}^n\left(\mathbf{v}, \lambda_h^n\right) \\ &= m_{s,\varepsilon}^n\left(\mathbf{f}_h^n, \mathbf{v}\right) + \frac{Re}{2\,\Delta t} m\left(4\mathbf{u}_h^{n-1} o X_2^{n-1} - \mathbf{u}_h^{n-2} o X_2^{n-2}, \mathbf{v}\right), \qquad (17a) \\ &b_1\left(\mathbf{u}_h^n, q\right) = 0, \qquad (17b) \\ &b_{2,\varepsilon}^n\left(\mathbf{u}_h^n, \mu\right) = 0. \qquad (17c) \end{aligned}$$

for all $\mathbf{v} \in \mathbb{V}_h(0)$, $q \in X_h$ and $\mu \in X_h$. The previous finite-dimensional linear system involves the following matrix structure:

$$\begin{pmatrix} A & B_1^T & B_2^T \\ B_1 & 0 & 0 \\ B_2 & 0 & 0 \end{pmatrix}$$

Such systems have been extensively studied and various efficient strategies are known (see e.g. [21]). In the present paper, this system is solved efficiently by the preconditioned conjugate gradient algorithm, as implemented in the Rheolef C++ library [49].

Summarising, the previous discrete algorithm envolves a semi-implicit numerical scheme with respect to time : its convergence with respect to the time step choice will be investigated in the third part of this paper. However, in the forthcomming section (3.4). this algorithm will be improved, turning to an implicit scheme.

3.3 The transport subproblem

3.3.1 Redistanciation

Due to the inextensibility of the vesicle membrane and the fluid incompressibility, the level set function ϕ, initially chosen to be a signed distance, remains also, for any $t > 0$, a signed distance among the advection step, as shown in appendix B. Nevertheless, after time and space discretization, we experimented that the approximation ϕ_h is no more a signed distance after the discrete counterpart of the advection step. As a consequence, an auxiliary problem called the *redistance problem* has to be solved in order to keep the function ϕ_h as a signed distance. The redistance step was detailed by the authors in a separate paper [36] and we recall here briefly the main idea. For all $t \in]0, T[$, an advection problem depending on a pseudo-time τ is introduced and we shall find its stationary solution. Let $\tilde{\phi}(t, .)$ be the known level set function at time t that is no more a distance function. The redistance problem writes:

$$\left\{ \begin{array}{rll} \dfrac{\partial \psi}{\partial \tau}(\tau, x; t) + \mathbf{v}.\nabla\psi & = \operatorname{sgn}\left(\tilde{\phi}\,(t, x)\right) + \lambda(\tau, x : t)\, g(\psi) & \text{a.e. } (\tau, x) \in]0, +\infty[\times\Lambda, \\ \psi(0, x; t) & = \tilde{\phi}(x, t) & \text{a.e. } x \in \Lambda. \end{array} \right. \tag{18}$$

where the advection vector field is $\mathbf{v} = \operatorname{sgn}\left(\tilde{\phi}\right) \dfrac{\nabla\psi}{|\nabla\psi|}$ and $\operatorname{sgn}\left(\tilde{\phi}\right)$ denotes the sign function and is equal to $0, -1, +1$ respectively on $\partial\Omega(t)$, inside $\Omega(t)$ and outside $\Omega(t)$. Notice also that $\lambda(\tau, x; t)$ is a Lagrange multiplier that enforces the constraint of constant volume locally at $x \in \Lambda$. The zero level set is not modified by the presence of λ in the right hand side of (18). This multiplier was first introduced by Sussman and Fatemi [51] in a finite difference context and then extended in [36] in a finite element context.

We chose $g(\psi) = \delta(\psi)|\nabla\psi|$, the Lagrange multiplier has an explicit average value $\lambda_{\mathcal{V}}$ over an arbitrary *finite volume* $\mathcal{V} \subset \Lambda$:

$$\lambda_{\mathcal{V}}(\tau; t) \quad = \quad \left\{ \begin{array}{ll} \dfrac{\int_{\mathcal{V}} \delta(\psi)\, \left(\mathbf{v}.\nabla\psi - \operatorname{sgn}\left(\tilde{\phi}\right)\right)\, \psi x}{\int_{\mathcal{V}} \delta(\psi)\, g(\psi)\, \mathrm{d}x} & \text{when } \mathcal{V} \cap \partial\Omega(t) \neq \emptyset \\ 0 & \text{otherwise} \end{array} \right. \tag{19}$$

The stationary solution satisfies $|\nabla\psi| = 1$ almost everywhere in Λ, consequently $\psi(\infty, .; t)$ is a signed distance and is taken as the new level set function $\phi(t, .)$ at time t. Let us notice that the solution ψ of the redistance problem (18) preserve the position of $\partial\Omega(t)$: for any $\tau > 0$, the zero level set of $\psi(\tau, .; t)$ is the same zero level set of $\phi(t, .)$. As a result the volume meas$(\Omega(t))$ is also preserved, this point has great importance for numerous applications. However, after discretization by finite difference or finite element methods, this property is satisfied only approximately. Let us introduce the `redistance` operator defined by $\phi(t, .) = \texttt{redistance}(\tilde{\phi}(t, .))$.

Let $\tilde{\phi}^n$ be the approximation of $\tilde{\phi}(t)$, at time t^n and $\psi^m, \mathbf{v}^m$ be approximations of $\psi(\tau), \mathbf{v}(\tau)$ respectively at τ^m. The time discretization is performed by using the method of characteristics and the total derivative $D\psi/Dt$ is approximated by a first-order backward Euler scheme as previously. The redistance problem (18) is solved explicitly:

$$\psi^{m+1} = \begin{cases} \psi^m & \text{when } |\tilde{\phi}^n| < \varepsilon \\ \psi^m \circ X^m_{\mathbf{v}_\varepsilon} + \Delta\tau \ \mathrm{sgn}_\varepsilon(\tilde{\phi}^n) & \text{otherwise} \end{cases} \tag{20}$$

Here, the characteristics have subscripts $\mathbf{v}_\varepsilon$ in order to avoid confusion. Let W_h be the space of piecewise constant functions on $\mathcal{T}_h$ and π_h denotes the Lagrange interpolation in Q_h. Let $\psi^0_h = \tilde{\phi}^{n+1}_h$. At any step $m \geq 0$ of the redistance algorithm, suppose $\psi^m_h \in Q_h$ being known, and let $\mathbf{g}^m_h \in Q^d_h$ be the approximation of $\nabla\psi^m_h \in W^d_h$ defined by the following linear system:

$$\int_\Lambda \mathbf{g}^m_h . \boldsymbol{w}_h \, \mathrm{d}x = \int_\Lambda \nabla\psi^m_h . \boldsymbol{w}_h \, \mathrm{d}x, \quad \forall \boldsymbol{w}_h \in Q^d_h$$

A mass lumping procedure is used for this linear system: the integrals involved in the computation of the coefficients of the matrix associated to the L^2 scalar product are evaluated by using the trapeze quadrature formula. By this way, the matrix of the linear system is replaced by a diagonal one, and the computation of $\mathbf{g}^m_h$ becomes explicit. Then, let

$$\mathbf{v}^m_{\varepsilon,h} = \pi_h \left(\mathrm{sgn}_\varepsilon \left(\tilde{\phi}^{n+1}_h \right) \frac{\mathbf{g}^m_h}{|\mathbf{g}^m_h|} \right)$$

Finally, the discrete version of the redistance algorithm writes also explicitly:

$$\psi^{m+1}_h = \begin{cases} \psi^m_h & \text{when } |\tilde{\phi}^n_h| < \varepsilon \\ \pi_h \left\{ \psi^m_h \circ X^m_{\mathbf{v}_\varepsilon} + \Delta\tau \ \mathrm{sgn}_\varepsilon(\tilde{\phi}^n_h)(1 - |\nabla\psi^m_h|) \right\} & \text{otherwise} \end{cases} \tag{21}$$

3.3.2 Improvement of the area and perimeter conservations

Let us summarize here the resolution of the problem:

Algorithm 1

- $n = 0$: Let $\partial\Omega(0)$ be the initial shape and ϕ_h^0 be its associated signed distance function. Let $\mathbf{u}_h^0 = \mathbf{u}_h^{-1} \in \mathbb{V}(\mathbf{u}_b)$ be the initial velocity field.
- $n \geq 1$: Let $\phi_h^{n-1} \in Q_h$ and $\mathbf{u}_h^{n-1}$, $\mathbf{u}_h^{n-2} \in \mathbb{V}_h(\mathbf{u}_b)$ being known. Then

  step 1 : compute $\tilde{\phi}_h^n = \pi_h \left(\phi_h^{n-1} \circ X_1^{n-1}\right) \in Q_h$;

  step 2 : compute $\phi_h^n = \texttt{redistance}(\tilde{\phi}_h^n)$;

  step 3 : compute $\mathbf{u}_h^n$, p_h^n and λ_h^n from (17).

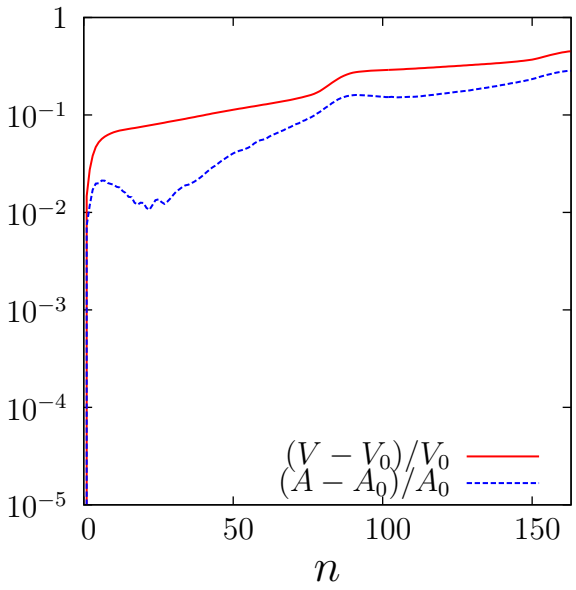

Figure 2: Without conservation improvement, the vesicle area and perimeter errors diverge: computations for $h = 5.3 \times 10^{-2}$, $\Delta t = 3 \times 10^{-2}$, $\tau = 0.81$ and $\varepsilon = 2.5\, h$.

In this section we present a numerical simulation to illustrate the features of the numerical method. We choose $Re = 10^{-3}$, $Ca = 10^3$, $\alpha = 1/10$, $\tau = 0.81$ and a viscosity ratio $\beta = 50$. Fig. 2 plots the evolution of the relative error in vesicle area and perimeter. Observe that, after few iterations, the error becomes higher than 10% of the reference vesicle area and perimeter: this error completely changes the vesicle shape, that evolves to a circular one. The algorithm must be modified in order to improve the area and perimeter conservation. The problem

of advection (4a) is substituted by the equivalent system:

$$\frac{\partial \phi}{\partial t} + \left[\mathbf{u} + (p_* + \lambda_* f)\,\mathbf{n}\right].\nabla\phi = 0 \quad \text{a.e } (t,x) \in]0,+\infty[\times\Lambda\,, \tag{22a}$$

$$\frac{\mathrm{d}}{\mathrm{d}t}\int_\Lambda (1-\mathscr{H}(\phi))\,\mathrm{d}x = 0 \quad \forall t \in]0,+\infty[\,, \tag{22b}$$

$$\frac{\mathrm{d}}{\mathrm{d}t}\int_{\partial\Omega} \mathrm{d}s = 0 \quad \forall t \in]0,+\infty[\,, \tag{22c}$$

where p_* and λ_* are two global Lagrange multipliers associated to two additional constraints for area and perimeter preservation. This system leads, after time discretization, to a modified and more robust scheme, with a modified advection field $\mathbf{u}_* = \mathbf{u} + (p_* + \lambda_* f)\,\mathbf{n}$. The variation of area $V(t)$ at time t^n writes:

$$\frac{\mathrm{d}V}{\mathrm{d}t}(t^n) = \left[\frac{\mathrm{d}}{\mathrm{d}t}\int_\Lambda (1-\mathscr{H}(\phi))\,\mathrm{d}x\right]_{t=t^n} = \frac{V^n - V^{n-1}}{\Delta t} + \mathcal{O}(\Delta t)\,, \tag{23}$$

where $V^{n-1} = \int_{\Omega^{n-1}} \mathrm{d}x$ is known and we want to impose that $V^n = V_0$ the initial area, in order to avoid the previous area error accumulation. Conversely, the variation of the perimeter $A(t)$ at time t^n expresses:

$$\frac{\mathrm{d}A}{\mathrm{d}t}(t^n) = \left[\frac{\mathrm{d}}{\mathrm{d}t}\int_{\partial\Omega} \mathrm{d}s\right]_{t=t^n} = \frac{A^n - A^{n-1}}{\Delta t} + \mathcal{O}(\Delta t)\,, \tag{24}$$

where $A^{n-1} = \int_{\partial\Omega^{n-1}} \mathrm{d}s$ is known and we want to impose that $A^n = A_0$ the initial perimeter. Combining (22a) and (22b), we obtain:

$$\frac{\mathrm{d}}{\mathrm{d}t}\int_\Lambda (1-\mathscr{H}(\phi))\,\mathrm{d}x = -\int_\Lambda \frac{\partial\phi}{\partial t}\delta(\phi)\,\mathrm{d}x = -\int_{\partial\Omega}\frac{1}{|\nabla\phi|}\frac{\partial\phi}{\partial t}\,\mathrm{d}s = \int_{\partial\Omega}\frac{1}{|\nabla\phi|}\mathbf{u}_*.\nabla\phi\,\mathrm{d}s\,. \tag{25}$$

Recall that, for any function φ and vector field $\mathbf{v}$, the Reynolds formula on a surface $\partial\Omega$ writes:

$$\frac{\mathrm{d}}{\mathrm{d}t}\int_{\partial\Omega} f\,\mathrm{d}s = \int_{\partial\Omega}\frac{\mathrm{d}f}{\mathrm{d}t} + \nabla.(f\,\mathbf{u}) - f(\nabla\mathbf{u}.\mathbf{n}).\mathbf{n}\,\mathrm{d}s\,. \tag{26}$$

With $\varphi = 1$ and $\mathbf{v} = \mathbf{u}_*$, and using the Green formula (8), we get successively:

$$\frac{\mathrm{d}}{\mathrm{d}t}\int_{\partial\Omega}\mathrm{d}s = \int_{\partial\Omega}\mathrm{div}_s\,\mathbf{u}_*\,\mathrm{d}s = \int_{\partial\Omega} H\,\mathbf{u}_*.\mathbf{n}\,\mathrm{d}s. \tag{27}$$

At time t^n, replacing $\mathbf{u}_*^n$ by $\mathbf{u}^n + (p_*^n + \lambda_*^n f)\,\mathbf{n}^n$ in (23)-(24) and using (25)-(27), we obtain the following linear system with two unknowns $(p_*^n, \lambda_*^n) \in \mathbb{R}^2$:

$$\begin{aligned} p^*\int_{\partial\Omega}\mathrm{d}s + \lambda^*\int_{\partial\Omega} f\,\mathrm{d}s &= \frac{V_0 - \int_{\Omega^n}\mathrm{d}x}{\Delta t} - \int_{\partial\Omega}\mathbf{u}.\mathbf{n}\,\mathrm{d}s\,, \\ p^*\int_{\partial\Omega} H\,ds + \lambda^*\int_{\partial\Omega} H\,f\,\mathrm{d}s &= \frac{A_0 - \int_{\partial\Omega^n}\mathrm{d}s}{\Delta t} - \int_{\partial\Omega} H\,\mathbf{u}.\mathbf{n}\,\mathrm{d}s\,. \end{aligned}$$

Choosing f a non-constant function ensure that this system is well-posed. In our simulations, we use $f(x_1,x_2) = 2x_1^2 + x_2^2$.

3.3.3 Improvement by mesh adaptation

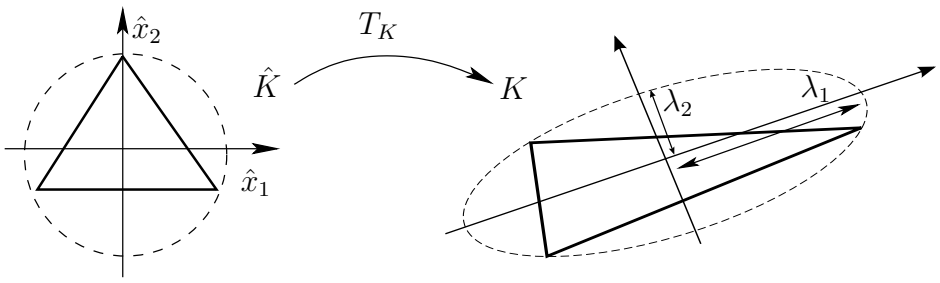

Figure 3: Transformation from the reference element $\hat{K}$ to any triangle K.

A way to adapt the mesh to the computation of a governing field is to equidistribute its interpolation error, i.e. to make it constant over all triangles and in the directions of maximal and minimal stretching and to adjust the maximal and minimal directions of stretching to others of maximal and minimal error. Our approach bases on the bidirectional anisotropic mesh generator `bamg` developed by F. Hecht [24] (see also [49, 26, 27]), together with the choice of a particular metric, specific to our time-dependent level set problem.

For any triangle K of the mesh $\mathcal{T}_h$ at time t, let T_K be the affine transformation which maps the reference triangle $\hat{K}$ into K (see Fig. 3):

$$\begin{array}{rccl} T_K: & \hat{K} & \longrightarrow & K \\ & \hat{x} & \longmapsto & \mathbf{x} = T_K(\hat{\mathbf{x}}) = M_K \hat{\mathbf{x}} + \mathbf{t}_K\,. \end{array}$$

where M_K is the Jacobian of T_K. Notice that M_K is unsymmetric and invertible, otherwise K would be flat. Thus, M_K admits a singular value decomposition (for SVD, see [23, p. 69]): $M_K = R_K^T \Lambda_K P_K$, where R_K and P_K are orthogonal and where Λ_K is diagonal with positive entries. The choice of the reference triangle $\hat{K}$ is not unique. It is common practice to choose as $\hat{K}$ the right triangle $\{(x_1, x_2), x_1 > 0, x_2 > O, x_1 + x_2 < 1\}$. For mesh generation and adaption purposes, an equilateral triangle, inscribed in the unit circle, is often preferred [20]. Since $\hat{x} = M_K^{-1}(x - t_K)$, the unit circle equation $\hat{x}^T \hat{x} = 1$ becomes:

$$1 = (x - t_K)^T M_K^{-T} M_K^{-1} (x - t_K) = (x - t_K)^T R_K^T \Lambda_K^{-2} R_K (x - t_K)$$

This is the equation of an ellipse containing K (see Fig. 3).

Following [24], our choice of the metric is based on the Hessian tensor of a specific governing field χ, for which we aim at decreasing the interpolation error. The interpolation error in the direction $\mathbf{v} \in \mathbb{R}^2$ is given by:

$$e_{K,\mathbf{v}} = h_{K,\mathbf{v}}^2 \left\| \frac{\partial^2 \chi}{\partial \mathbf{v}^2} \right\| \quad \text{on } K,$$

where $h_{K,\mathbf{v}}$ denotes the length of K in the direction $\mathbf{v}$ and $\dfrac{\partial^2 \chi}{\partial \mathbf{v}^2} = \mathbf{v}^T \, \nabla\nabla\chi \, \mathbf{v}$, and $\nabla\nabla\chi$ is the Hessian matrix of χ.

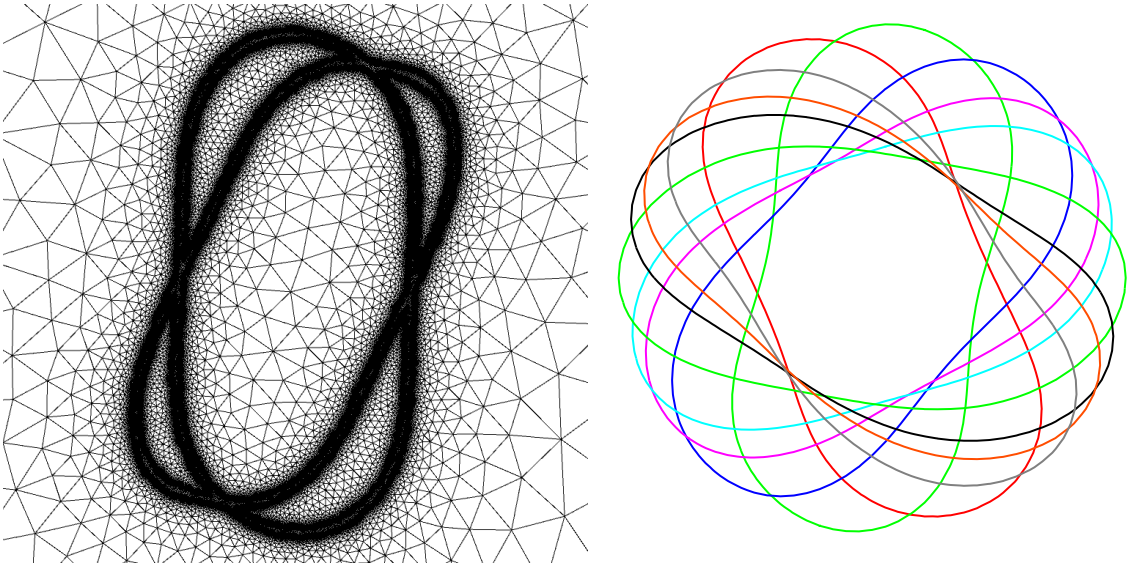

Figure 4: (left) Zoom on the adapted mesh ; (right) Vesicle tumbling under a linear shear flow for $Re = 10^{-3}$, $Ca = 10^4$, $\alpha = 1/4$, $\beta = 20$ and $\gamma = 0.89$. The shapes are shown for $t = kT_p/14$, $k \in \{1, 2, 3, 4, 5, 8, 11, 12, 13\}$, where $T_p = 10.3$ is the tumbling period.

By adjusting the directional sizes $h_{K,\mathbf{v}}$ of K for each eigenvector of the Hessian matrix and each element K, the local directional interpolation errors can be equidistributed on the whole domain. An adaptation loop is required in order to guarantee the convergence of both the approximation of χ and its corresponding mesh. In order to adapt the mesh to the vesicle boundary $\partial\Omega^n$ at each time step t_n, the governing field $\chi = \delta_\varepsilon(\phi^n) + \delta_\varepsilon(\phi^{n-1})$ has been chosen for the adaptation loop. For a uniform mesh, the regularization parameter used for the computation of integrals over $\partial\Omega$ is chosen as proportional to the element size: $\varepsilon = 2h$. This choice is extended to a non-uniform mesh with a non-constant $\varepsilon(x)$, $x \in \Lambda$, that is proportional to an average value of the local mesh size: $\varepsilon(x) = 2\sqrt{2}\,\mathrm{meas(K)}^{\frac{1}{2}}$, for all $x \in K$. Fig. 4.a shows a zoom on the adapted mesh at the end of the adaptation loop, where both the contours of $\partial\Omega^{n-1}$ and $\partial\Omega^n$ are captured. Fig. 4.b represents the vesicle boundary evolution, as computed by the present auto-adaptive procedure.

3.4 Implicit time splitting algorithm

In order to deal efficiently with the highly nonlinear term expressing the Helfrich force, a fixed point algorithm variant is introduced between the two main steps of the previous algorithm: (i) first, the nonlinear dynamics is solved for fixed level set function and membrane geometry description; (ii) fecond, the advection and redistance subproblem are solved for a fixed fluid velocity. This fixed point iteration is repeated until the relative error is less than a given tolerance ϵ_{fp}, choosen here as 10^{-6} for the practical computations. This strategy has the advantage to split the problem into a succession of two simpler, linear and more standard subproblems, while maintaining a robust implicit algorithm.

Algorithm 1 Implicit time splitting algorithm

Let $n = 0$ and $(\mathbf{u}_h^0, \varphi_h^0)$ be the known initial condition
for $n = 1, \ldots, n_{\max} = T/\Delta_t$ **do**
  Let $(\mathbf{u}_h^{n+1,0}, \varphi_h^{n+1,0}) = (\mathbf{u}_h^n, \varphi_h^n)$ being known
  for $k = 0, \ldots, k_{\max}$ **do**
    Let $(\mathbf{u}_h^{n+1,k}, \varphi_h^{n+1,k})$ being known
    compute the discrete Canham-Helfrich force $f_h^{n,k+1}$ from $\varphi_h^{n+1,k}$
    solve the following linear generalised Stokes subproblem:
    find $\mathbf{u}_h^{n+1,k+1} \in \mathbb{V}_h(\mathbf{u}_b)$, $p_h^{n+1,k+1}$ *and* $\lambda_h^{n+1,k+1} \in X_h$ *such that*

$$\begin{aligned}
&\frac{3Re}{2\Delta t} m\left(\mathbf{u}_h^{n+1,k+1}, \mathbf{v}\right) + a_\varepsilon^{n+1,k+1}\left(\mathbf{u}_h^{n+1,k+1}, \mathbf{v}\right) + b_1\left(\mathbf{v}, p_h^{n+1,k+1}\right) \\
&\quad + b_{2,\varepsilon}^{n+1,k+1}\left(\mathbf{v}, \lambda_h^{n+1,k+1}\right) = m_{s,\varepsilon}^{n+1,k+1}\left(\mathbf{f}_h^{n+1,k+1}, \mathbf{v}\right) \\
&\quad + \frac{Re}{2\,\Delta t} m\left(4\mathbf{u}_h^{n+1,k} oX_2^{n+1,k} - \mathbf{u}_h^{n+1,k-1} oX_2^{n+1,k-1}, \mathbf{v}\right), \ \forall \mathbf{v} \in \mathbb{V}_h(0) \\
&b_1\left(\mathbf{u}_h^{n+1,k+1}, q\right) = 0, \ \forall q \in X_h \\
&b_{2,\varepsilon}^{n+1,k+1}\left(\mathbf{u}_h^{n+1,k+1}, \mu\right) = 0, \ \forall \mu \in X_h
\end{aligned}$$

    solve the modified advection system (22)
    compute the signed distance function $\varphi_h^{n+1,k+1}$ following (21)
    if $\|\mathbf{u}_h^{n,k+1} - \mathbf{u}_h^{n,k}\|_{1,\Lambda} \leq \varepsilon_{\text{fp}} \|\mathbf{u}_h^{n,k}\|_{1,\Lambda}$ **then**
      set $(\mathbf{u}_h^{n+1}, \varphi_h^{n+1}) = (\mathbf{u}_h^{n+1,k+1}, \varphi_h^{n+1,k+1})$
      stops the k loop
    end if
  end for
  compute the new adapted mesh as described in section 3.3.3
end for

4 Numerical results

In this section, we provide several numerical tests carried out with the finite element level set approach previously described. The algorithms employed in the simulations have been implemented using a free software, the finite element library Rheolef [49]. Simulations show, in accord with literature, that two flow regimes exist: a steady-state *tank-treading* regime where the vesicle assumes a steady-state shape and its inclination angle remains constant with time, while the fluid membrane treads as a tank and the internal fluid follows this rotation. The second regime is a periodic *tumbling* one, where the vesicle shape rotates. The transition between the two regimes for a vesicle of fixed reduced area γ happens at a critical viscosity ratio between the inside and outside fluid, beyond which the vesicle tumbles. In order to validate the proposed method, we compared our results with available numerical data, i.e. for small Reynolds number. We have determined the transition line separating the two regimes. These results are also founded to be in good agreement with the phase field method presented in [5] (see also Fig. 2 in [37] for a comparison). Note that both the tank treading and tumbling motions are observed experimentally (see e.g. Kantsler and al. [30]).

4.1 Vesicles in the tumbling mode

The small Reynolds number case is considered in this paragraph: this is a typical situation in microfluidic devices and the viscous forces are dominant over the inertial ones: the flow is almost laminar, and no turbulence can be observed, at least in the absence of vesicle. The following parameters are chosen: $Re = 10^{-4}$, $Ca = 10^3$ and a vesicle with a reduced area $\gamma = 0.89$. The time step is $\Delta t = 2.5 \times 10^{-3}$. In their experimental tests, Vitkova and al. [52] use vesicles with a diameter $50\,\mu$m in a pipe with a length 1 mm. This leads to a confinement equal to 1/20: In the present simulations, confinements between 1/2 and 1/5 was used when using an uniform mesh, and up to 1/12, in the case of an adapted mesh. Remark that the viscosity ratio β is chosen such that the vesicle is in a tumbling mode.

Mass preservation – First, let us check the improvement of the area and perimeter conservation, as introduced in the procedure of the previous section. Computations are first performed with $\alpha = 1/9$: Fig. 5 plot the evolution of relative mass errors $(V - V_0)/V_0$ and $(A - A_0)/A_0$. Observe that, over a duration equivalent to 80 periods of tumbling, both the area and perimeter relative errors remain bounded by 10^{-3}. The improvement of the conservation, based on Lagrange multipliers, is clearly shown by a comparison with the previous Fig. 2, where the errors diverge after the equivalent of two periods of the vesicle tum-

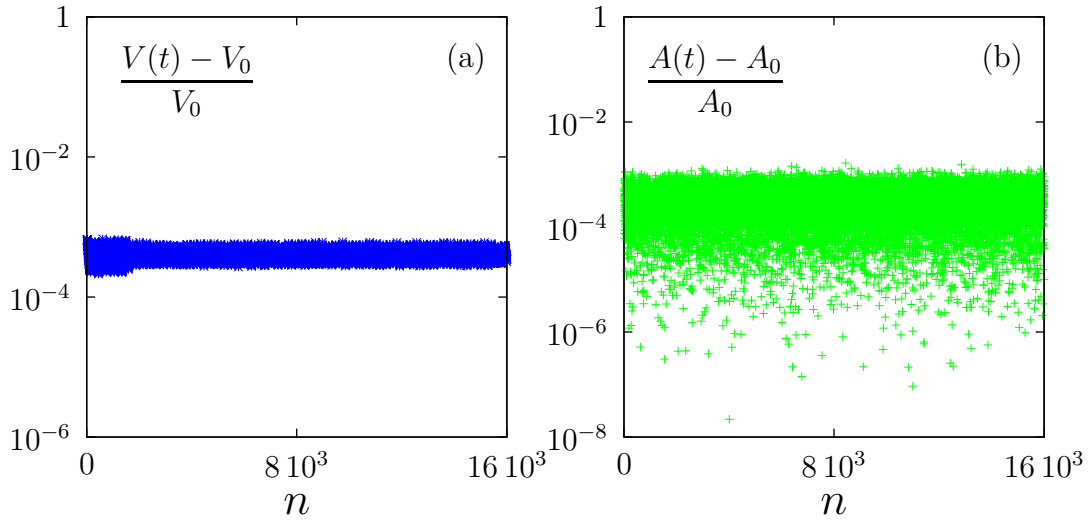

Figure 5: With conservation improvement, area and perimeter errors remains bounded: (a) the vesicle area error; (b) the vesicle perimeter error.

bling.

Dependance on the choice of f – Now, we investigate the effect of the choice of the function $f(x_1, x_2)$ (see (22a)) on the computation of the solution. Three expressions of f are tested: $f_1(x_1, x_2) = 2x_1^2 + x_2^2$, $f_2(x_1, x_2) = 2x_1^2 + 5x_2$ and $f_3(x_1, x_2) = 3x_1$. A vesicle with a reduced area $\gamma = 1$ keeps a circular shape while advected by the simple shear flow and the error between the numerical and the exact solution for the time interval $]0, 2s[$ is computed. The error upon the geometry is expressed by the L^2 norm of $\mathscr{H}_\varepsilon(\phi) - \mathscr{H}_\varepsilon(\phi_h)$ where ϕ and ϕ_h are respectively the exact and the computed level set functions, and $\mathscr{H}$ denotes the regularized Heaviside function, as introduced in section 3.2.3. This error is plotted for the three different expressions of f on Fig. 6.a. Observe that the error decreases versus the mesh size: thus, the choice of f doesn't affect the convergence of the method. Moreover, the plot suggests a $\mathcal{O}(h)$ convergence of the predicted geometry versus the mesh size.

Dependance upon the time step – Let us consider the case when the algorithm is not fully implicit : the fixed point loop is stopped after a first computation, i.e. $k_{\max} = 1$ in Algorithm 2. Due to the moving interface and the computation of the Helfrich forces, there exists a critical choice of the time step Δt_c such that for values beyond this threshold time step $\Delta t > \Delta t_c$ the algorithm is no more able to converge. Fig. 6.b plots Δt_c versus the mesh size h and one

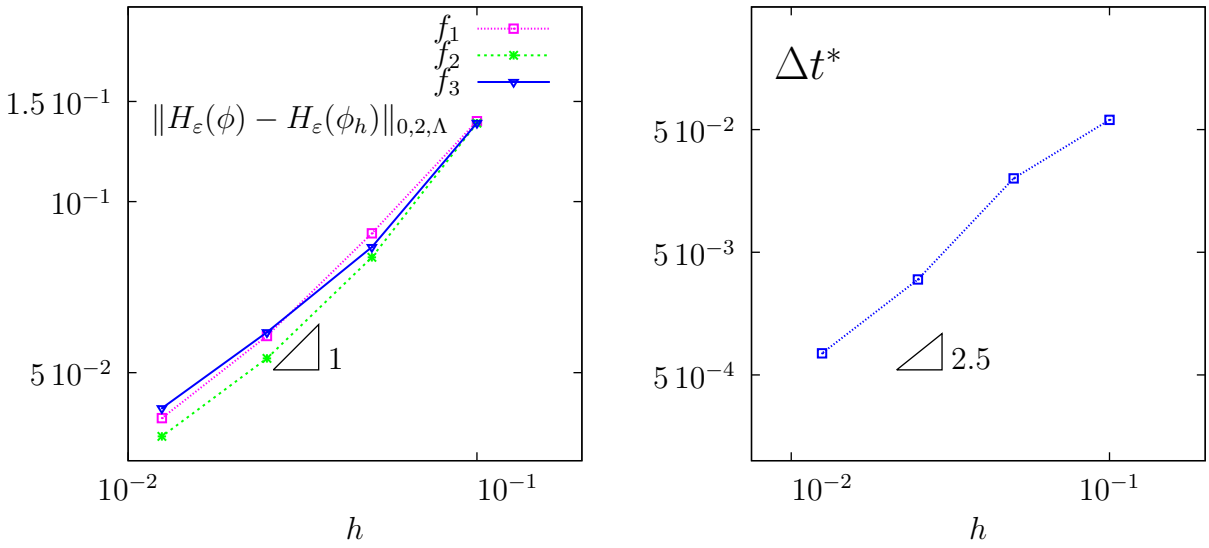

Figure 6: (a) Convergence properties for three expressions of f ($Re = 0.1$, $Ca = 10^4$ and $\beta = 75$). (b) Critical value of the time step in log-log scale for different mesh steps ($Re = 1$, $Ca = 10^4$, $\beta = 100$ and $\gamma = 0.95$).

can observe that the slope is of about 2: this suggests that Δt_c behaves as h^2. This time step limitation is related to the case of an explicit scheme : the use of an implict one appears to be of major importance, as there is no more limitation with Δt for the convergence of the algorithm.

Dependance on the confinement – Let us now investigate the effect of

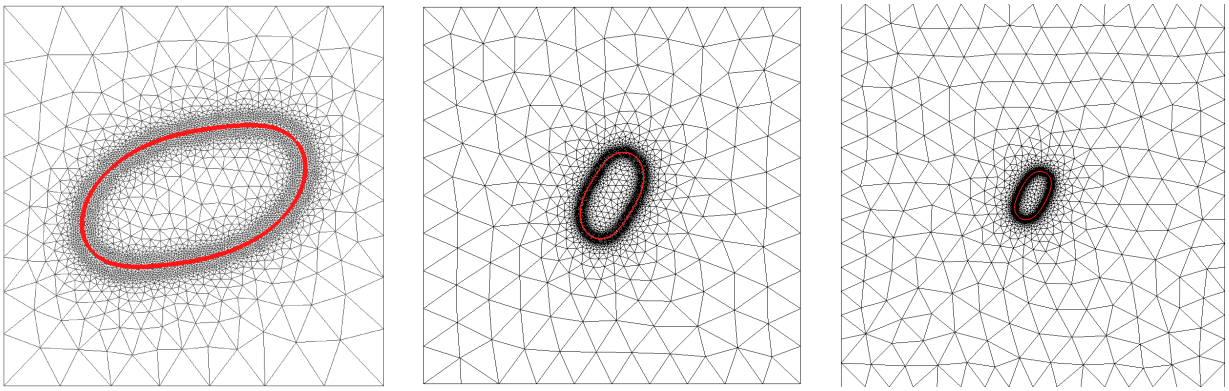

Figure 7: Adapted meshes used for the study of the effect of the confinement α: from left to right: $\alpha = 1/2$, $1/5$ and $1/9$.

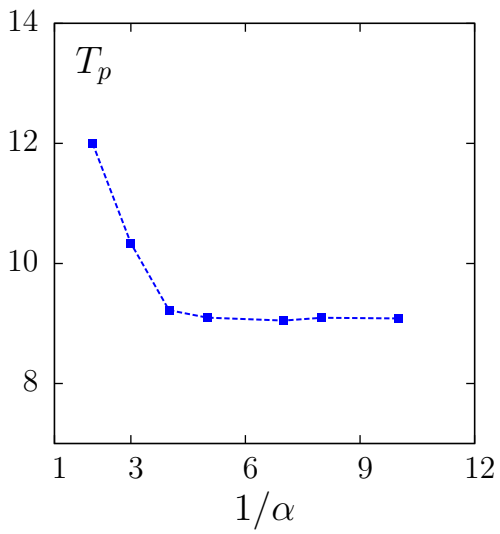

Figure 8: Tumbling regime: period T_p *vs* $1/\alpha$ for $Re = 10^{-4}$, $Ca = 10^3$, $\beta = 20$ and $\gamma = 0.82$.

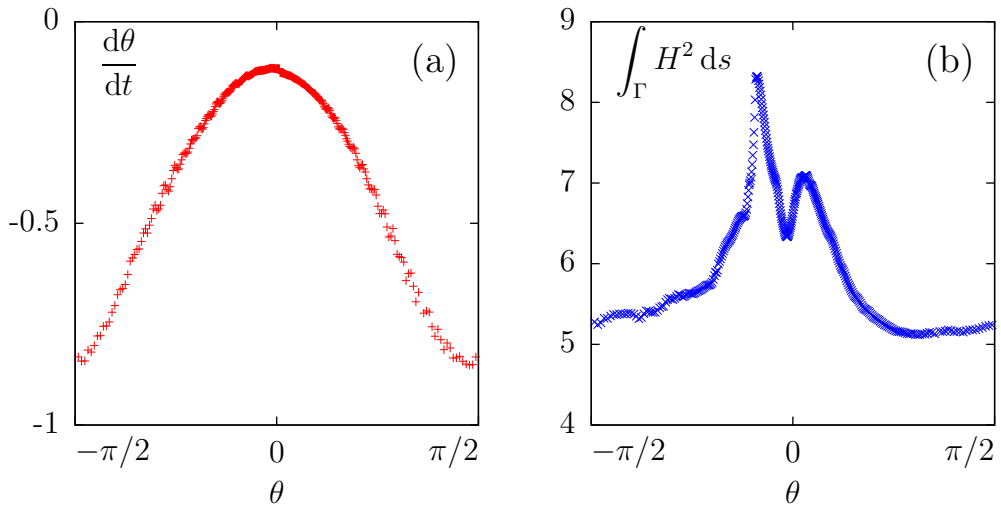

Figure 9: Tumbling regime: Lissajous curves: (a) the angular velocity $\frac{d\theta}{dt}$ *vs* θ and (b) the Canham-Helfrich energy *vs* θ. ($Re = 10^{-4}$, $Ca = 10^3$, $\alpha = 1/4$, $\beta = 20$ and $\gamma = 0.82$).

the confinement α on the tumbling regime of the vesicle : a recirculation flow around the vesicle membrane can change deeply the dynamics behaviour of the membrane. Adapted meshes, that capture the vesicle boundary are shown in Fig. 7 for different confinements. Fig. 8 plots the evolution of the tumbling

dimensionless period, denoted by T_p, versus $1/\alpha$. As expected, these results show that results depend strongly on the confinement α when α is close to one, i.e. when the vesicle is confined, while the tumbling period becomes independent for small α values. In the simulations presented in the rest of the paper, we choose $\alpha = 1/4$: this choice guaranties that the dynamics depends weekly upon the confinement.

Let us denote by $\theta(t)$ the inclination angle measured counterclockwise from the positive x_1 semi-axis. The numerical computation of the inclination angle $\theta(t)$ for an arbitrary shape $\Omega(t)$ is reported in appendix C. The vesicle reaches a periodic regime after about 10 periods of tumbling: the inclination angle $\theta(t)$ becomes periodic. Let us observe on Fig. 9 some Lissajous representations, suitable for periodic phenomenas. The solution is represented, during the 10^{th} period, where the periodic regime is well established. Fig. 9.a the angular velocity $\frac{d\theta}{dt}$ versus θ: observe that the angular velocity is minimal when $\theta = 0$, i.e. when the vesicle is aligned with the horizontal axis, while its maximal when the vesicle is aligned vertically ($\theta = \pm\pi/2$). Fig. 9.b the evolution of the Canham-Helfrich energy versus θ: this energy reaches a global maximum when the vesicle is roughly aligned horizontally and, conversely, reaches a minimum when its roughly aligned vertically. Here, there is a small phase shift: the extrema of the energy are slightly in advance with the corresponding extrema of the angular velocity.

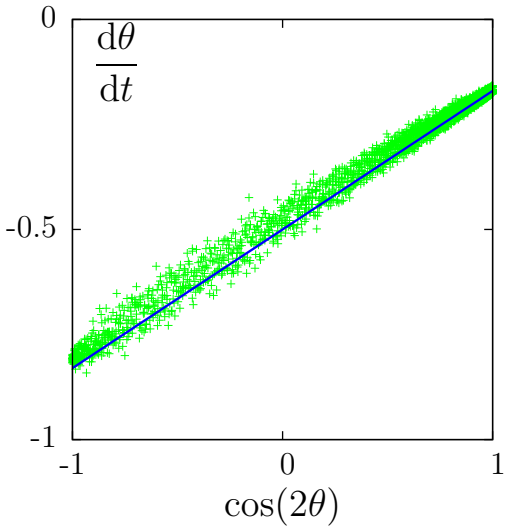

Figure 10: Tumbling regime: $\frac{d\theta}{dt}$ *vs* $cos(2\theta)$ for $Re = 10^{-4}$, $Ca = 10^4$, $\alpha = 1/9$, $\beta = 50$ and $\gamma = 0.84$. A linear regression leads to $\frac{d\theta}{dt} = 0.33\, cos(2\theta) - 0.5$, as indicated by the continuous line.

In order to study analytically the dynamics of vesicles, a rough analytical model was proposed in 1982 by Keller and Skalak [31]. This model incorporates a

quasi-inextensible membrane, but vesicles were treated as undeformable liquid ellipsoids. Nevertheless, this model was able to reproduce tumbling regime notably for reduced area γ near 1 (i.e. quasi-spherical shapes), for which the distance to inextensibility is weak. Keller and Skalak [31] showed that the ellipsoid motion is described by:

$$\frac{\mathrm{d}\theta}{\mathrm{d}t} = -\frac{1}{2} + c(\gamma\,,\,\beta)cos(2\theta),$$

where $c(\gamma\,,\,\beta)$ is a coefficient depending on the aspect ratio γ and the viscosity ratio β. Fig. 10 plots $\frac{\mathrm{d}\theta}{\mathrm{d}t}$ versus $cos(2\theta)$. Observe the good correspondence with the affine behavior, as predicted by the Keller and Skalak theory. A linear regression on the numerical simulation data leads to the slope coefficient $c = 0.33$.

Dependance on the reduced area – Let us turn to the effect of the reduced

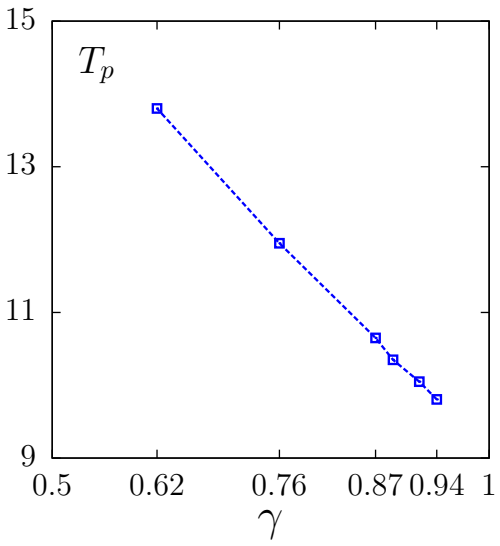

Figure 11: Tumbling regime: period T_p *vs* the reduced area γ, for $Re = 10^{-4}$, $Ca = 10^3$, $\alpha = 1/4$ and $\beta = 50$.

area γ on the period of tumbling T_p. We consider a vesicle with a viscosity ratio $\beta = 50$ in a shear flow with a Reynolds number $Re = 10^{-4}$ and a Capillarity number $Ca = 10^3$. Observe on Fig. 11 the quasi-linear dependence of T_p upon γ. This behaviour can be interpreted as follow: when the vesicle is more circular (e.g. for high reduced area), it is less deformed during the tumbling dynamics and its rotational mouvement is easier. As a consequence, the tumbling period becomes smaller.

4.2 The tank-treading regime

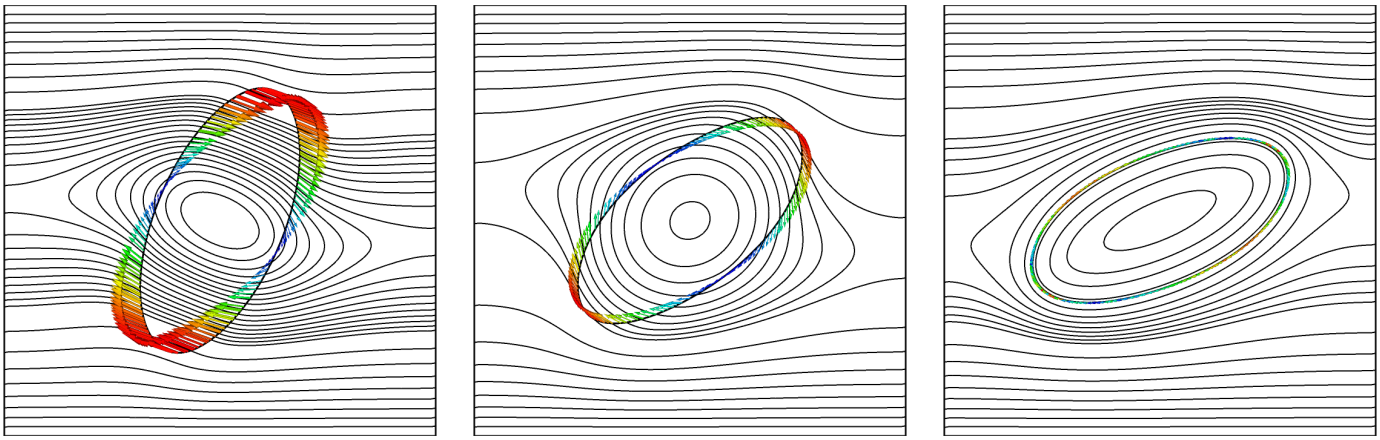

Figure 12: Tank-treading regime vs time for $Re = 10^{-4}$, $Ca = 10^4$, $\alpha = 1/2$, $\beta = 1$ and $\gamma = 0.84$: streamlines lines and velocity field on the vesicle membrane $\partial\Omega$. Figures are, from left to right, at $t = k\Delta t$, $k \in \{60, 120, 1000\}$ and $\Delta t = 2 \times 10^{-2}$.

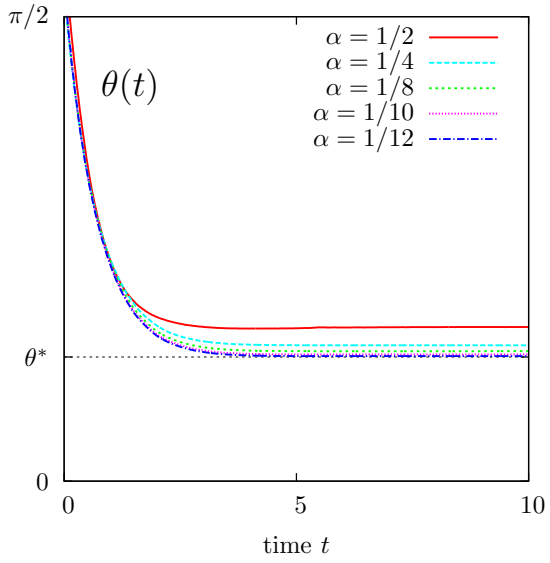

Figure 13: Tank-treading regime: time evolution of the tumbling inclinaison angle for various confinements α and $\gamma = 0.89$.

When the viscosity ratio β becomes smaller than a critical value, a transition to the tank-treading regime occurs. The fluid inside the vesicle is highly deformed and rotated, and the vesicle adopts a stationary boundary $\partial\Omega$. Fig. 12 plots the streamlines and the velocity fields on the vesicle membrane. Remark that,

when the stationary regime is reached, the velocity field become tangential to the membrane, and then we observe that the tank treading mouvement becomes more appropriate to preserve the minimal energy state. Fig. 13 represents the vesicle orientation $\theta(t)$: observe that it reaches rapidly a stationary value, denoted by θ^*. Notice that the velocity is not vanishing along $\partial\Omega$: the membrane continues to tread like a tank and the internal fluid follows this rotation.

h	dof	$\gamma = 0.8$	0.85	0.90	0.95
1/20	7082	0.3852	0.4700	0.5728	0.7506
1/30	15722	0.3701	0.4524	0.5562	0.7311
1/50	43202	0.3595	0.4356	0.5329	0.7157
1/70	84282	0.3552	0.4285	0.5219	0.7044
1/90	138962	0.3518	0.4234	0.5183	0.7004
extrapolation		0.3450	0.4189	0.5130	0.6901

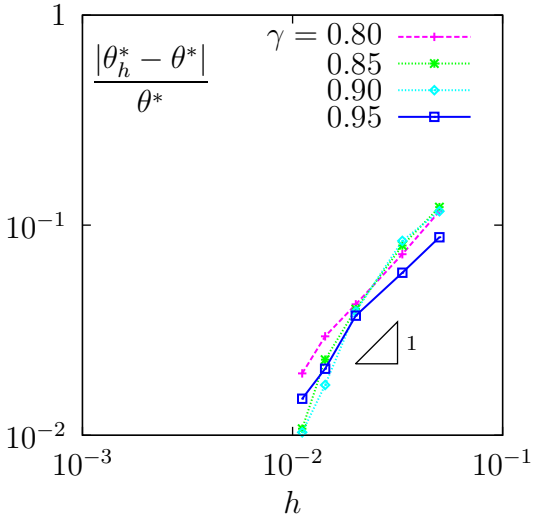

Figure 14: Tank-treading regime: convergence of the stationary angle θ^* versus the mesh refinement h.

$1/\alpha$	0.8	0.85	0.9	0.95
2	0.4301	0.5472	0.6300	0.8212
4	0.3951	0.4705	0.5546	0.7502
8	0.3615	0.4409	0.5224	0.7115
12	0.3518	0.4234	0.5183	0.7004
extrapolation	0.3412	0.4150	0.5114	0.6928

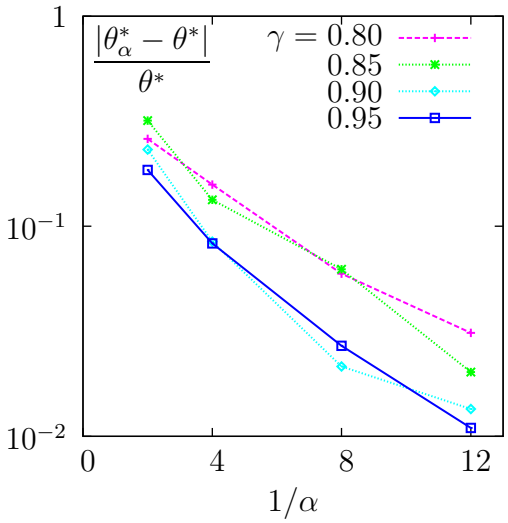

Figure 15: Tank-treading regime: convergence of the stationary angle θ^* versus the confinement $1/\alpha$.

Numerical validation – In this paragraph, we study the convergence properties of the numerical solution versus both the mesh refinement h and the confinement α. For this purpose, we perform a shear flow simulation of vesicles with several reduced areas γ following a tank treading motion. The convergence properties are evaluated by observing the dependence of the stready state inclinaison angle θ^* upon h and α.

Let us first consider the dependence upon the mesh refinement: a family of regular grids are considered. Fig 14 groups in a table the stationary angles θ_h^* obtained for decreasing values of h and for various reduced areas γ. By extrapolation for $h = 0$, we are able to compute an improved value of the stationnary angle, denoted simply as θ^*. Our extrapolation is based on a linear least square procedure, as implemented in [54]. Then, the error is estimated as $\theta_h^* - \theta^*$ and ploted on Fig. 14. Observe that the slope in logarithmic scale is of about one, suggesting a $\mathcal{O}(h)$ convergence.

Figure 15 groups in a table the stationary angles θ_α^* obtained for decreasing values of the confinement α and for various reduced areas γ. By a extrapolation at $\alpha = 0$, we compute an improved value of the stationnary angle, denoted simply as θ^* and estimate the error $\theta_\alpha^* - \theta^*$. The plot on Fig. 15 suggests an exponential convergence of the stationnary angle to a value associated to an unconfined vesicle.

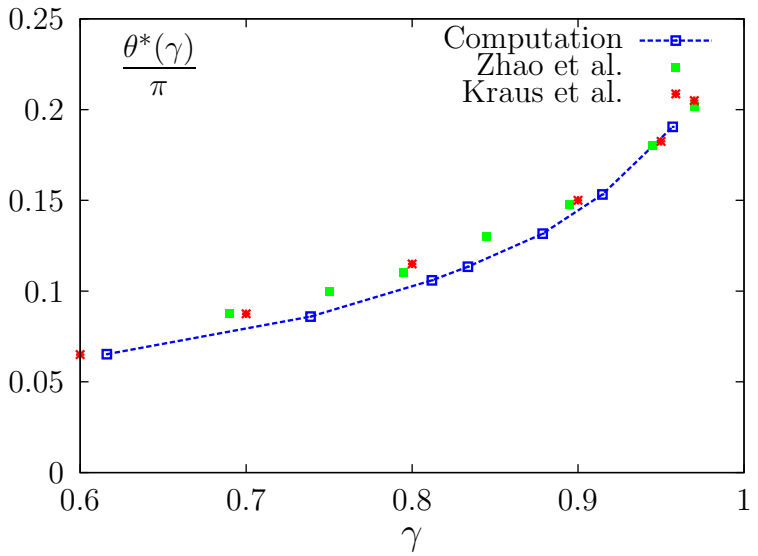

Figure 16: Inclinaison angle of the steady-state tank-treading regime with a viscosity ratio $\beta = 1$. Comparative study for $Ca = 10$ with nemerical results of Zhao et al. (2009) [55] for $Ca = 9$ and Kraus et al. (1996) [33] for $Ca = 10$.

Experimental validation: comparaison with data in vitro and simulations For accuracy raisons, we compare our results with those performed by Zhao et al. (2009) [55] and by Kraus et al. (1996) [33]. Then, in terms of physiological relevance, we compare with experiment measurments observed by Kantsler & Steinberg (2005) [30]. Firstly, we study the dynamics of vesicles in the tank treading regime for vesicles with different reduced areas and we perform a quantitative comparaison with the results presented in [55] and [33]. Then, by modifying the viscosity ratio, we perform simulations for $\beta \in 1, 2.7, 5.4$ and we proceed to a comparative study in light of experimental observations in [30] and numerical results in [55]. In both simulations and data, we observe from Figure 16 and Figure 17, by plotting the dependence of θ^* upon γ, a close fit of the simulated vesicle motion with respect to the experiments and numerical data. At this level, we note that, after this work was completed we found on the website a preprint by D. Salac and M. Miksis [48] treating the problem of vesicles with a level set method. We can observe that our results in Figure 16 fit with the ones performed in this work (see Fig.17 in [48]). In summary, we obtain a satisfactory agreement between numerical results and measured data.

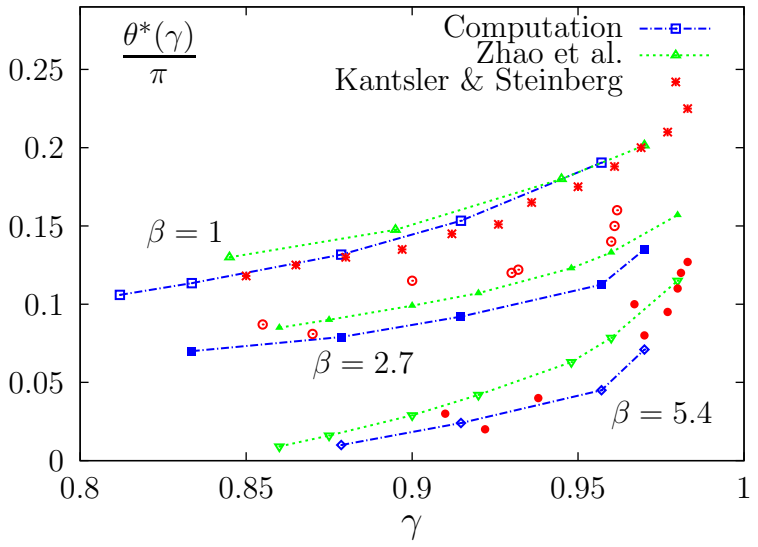

Figure 17: Inclinaison angle of the steady-state tank-treading regime with different viscosity ratio $\beta = 1$, $\beta = 2.7$ and $\beta = 5.4$: comparative study of our results (*datched blue line with squares*) with numerical results of Zhao et al. (2009) (*dotted green line with triangular symbols*), and experimental validation with the measurements of Kantsler & Steinberg (2005) [30] (*circular red point symbols*).

4.3 Effect of inertia

An exhaustive study of the rheology of a vesicle in the presence of inertia has been carried out in this section. Although the basic behaviors had already been observed, the results shown in this part were nontrivial and not completely understood yet. For red blood cells in blood vessel, the Reynolds number Re is not always very small so the Stokes limit is not always reached: R_0 is about 3×10^{-6} m η_0 is about 10^{-3} Pa.s and ρ is about 10^3 kg.m^{-3}. For a mean velocity in the blood vessel about 1 m.s^{-1}, the Reynolds number $Re \approx 3$. In laboratory experiments, with experimental vesicles, R_0 is about 5×10^{-5} m while we can supervise vesicles using rapid cameras that can reach a velocity of about 0.1 m.s^{-1}. In that case, the Reynolds numbers $Re \approx 5$. In both cases, the inertia effect can no more be neglected and the prediction of vesicle behaviors for these magnitude of the Reynolds number is of major importance. Moreover, we show in this paragraph, that inertia effects change dramatically the vesicle behavior for the simple shear flow.

Fig. 18 plots the evolution of the vesicle for $Re = 0.4$. Observe that the behavior, is dramatically different from the corresponding one for small Reynolds numbers, as shown previously on Fig. 4.b. Especially, deformations are more important when the inclination angle is close to $\pi/2$.

Above a critical value of the Reynolds number, the tumbling regime disappears: a new tank-treading regime occurs and the vesicle keeps a constant angle. Figs. 19.a and 19.b plot the angle $\theta(t)$ for $\gamma = 0.82$: observe that the period T_p increases with Re until a critical Reynolds number between 3.5 and 4. For $Re > 4$, the angle $\theta(t)$ becomes constant: the vesicle switch from a tumbling regime to a tank-treading one. More developments on the effect of the inertia, as phase diagram, can be found in [37].

5 Conclusion

The new level method presented in this paper for the simulation of the vesicle dynamics exactly satisfies both the inextensibility membrane condition and the volume conservation : these properties are also true at the discrete level, for the finite element solution. We show that the proposed method, based on Lagrange multipliers, solves a lack of precision problem when dealing with the inextensibility constraints and the level set method. Moreover, an automatic adaptive method, used at each time step, enhance the prediction of the vesicle motion. With this procedure, we are able to accurately reproduce the change of regime, from tank-treading to tumbling, as observed when the viscosity ratio varies.

We exhibit the apparition of a new change of regime when the Reynolds number

is below a critical value. Moreover, the critical Reynolds number of this order of magnitude for both red blood cells in arteries and vesicles used in laboratory experiments. In the future, new experiments on vesicle would be necessary to infirm or confirm your numerical predictions.

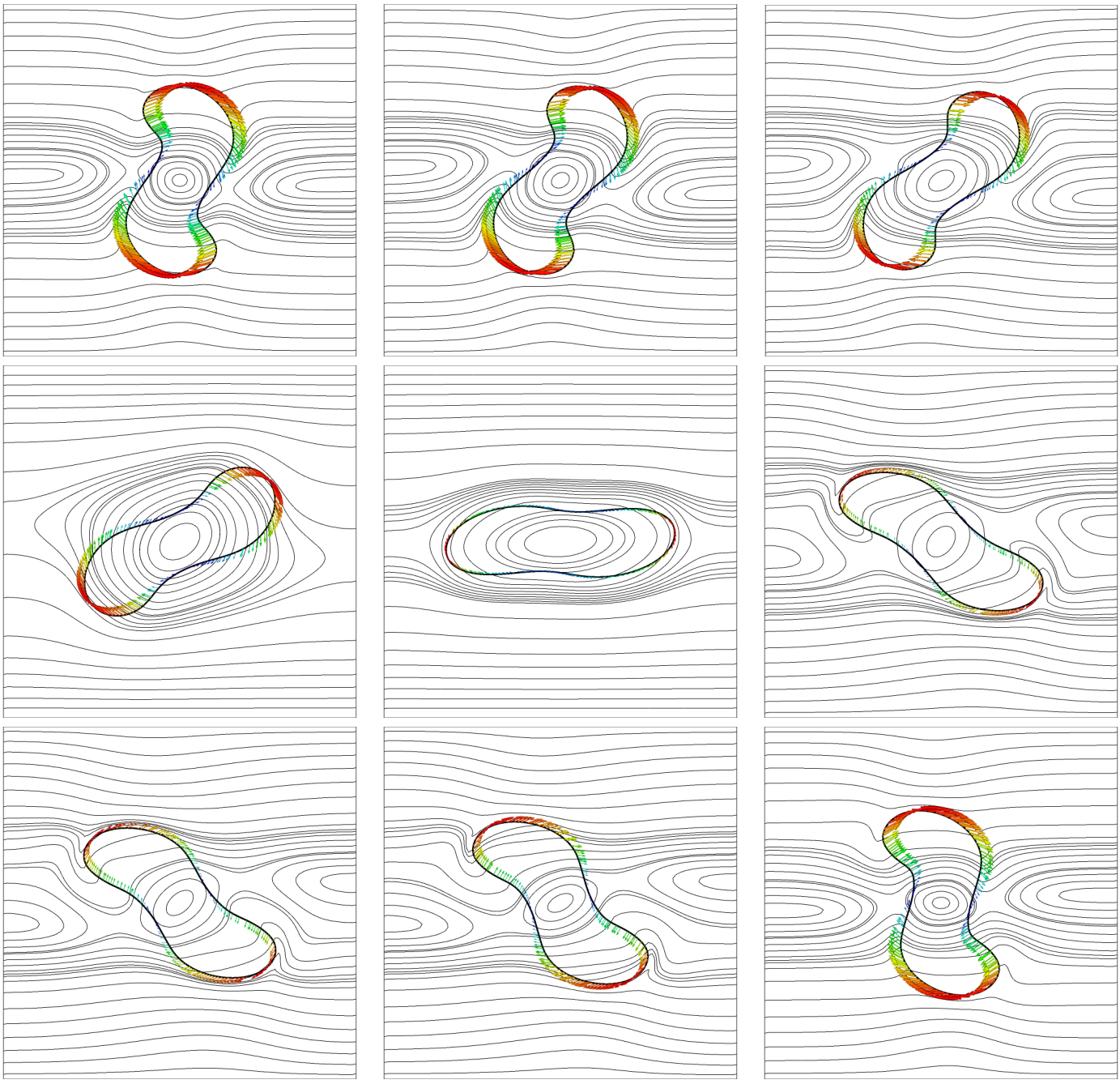

Figure 18: Inertia effects: streamlines lines and velocity field on the vesicle membrane for $Re = 0.4$, $Ca = 10^4$, $\alpha = 1/2$, $\beta = 10$ and $\gamma = 0.62$. Figure are shown, from left to right and top to bottom, at $t = kT_p/24$, $k \in \{2, 4, 6, 8, 13, 18, 20, 22, 24\}$, where $T_p = 29.1$ is the tumbling period.

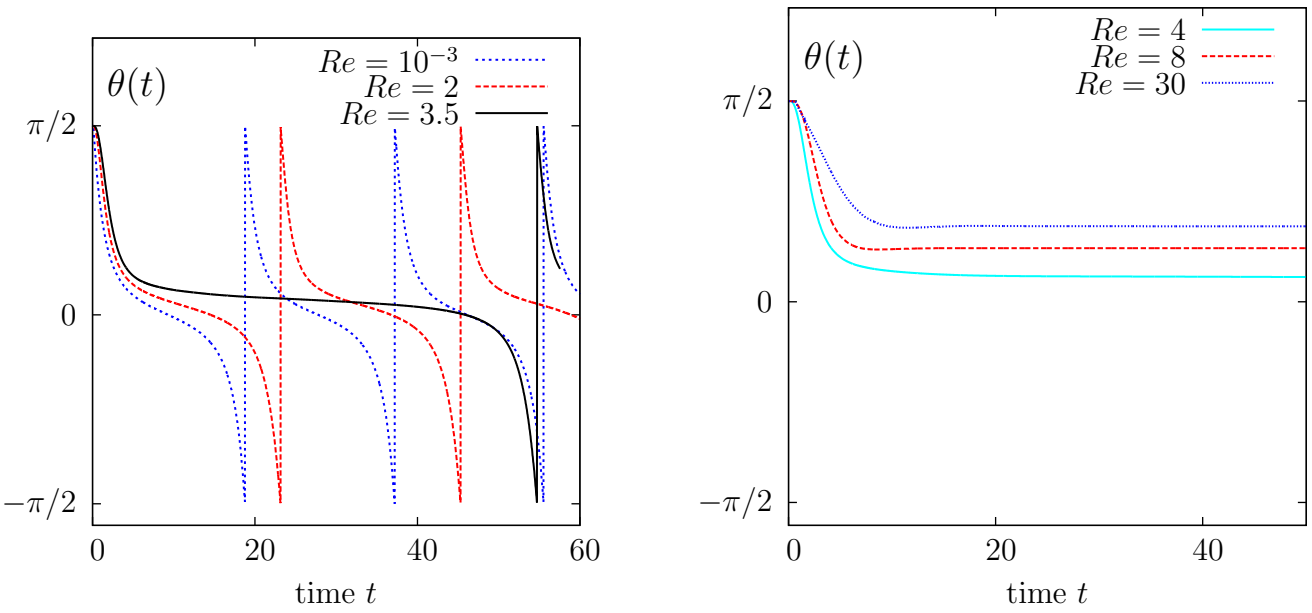

Figure 19: Inertia effect: influence of Re on the vesicle inclination $\theta(t)$ for $Ca = 10^4$, $\alpha = 1/2$, $\beta = 10$ and $\gamma = 0.82$. (a) tumbling regime when $Re \leq 3/5$; (b) tank-treading regime when $Re \geq 4$.

References

[1] R. A. Adams and J. J. F. Fournier. *Sobolev spaces*. Elsevier, second edition, 2003.

[2] S. M. Allen and J. W. Cahn. A microscopic theory for antiphase boundary motion and its application to antiphase domain coarsening. *Acta Metal.*, 27:1085–1095, 1979.

[3] G. Aubert and P. Kornprobst. *Mathematical problems in image processing. Partial differential equations and the calculus of variations*. Springer, second edition, 2006.

[4] J.W. Barrett, H. Garcke, and R. Nürnberg. Parametric approximation of Willmore flow and related geometric evolution equations. Technical Report 22/2007, Univ. Regensburg, Deustchland, 2007.

[5] J. Beaucourt, F. Rioual, T. Seon, T. Biben, and C. Misbah. Steady to unsteady dynamics of a vesicle in a flow. *Phys. Rev. E*, 69:011906, 2004.

[6] T. Biben, K. Kassner, and C. Misbah. Phase-field approach to three-dimensional vesicle dynamics. *Phys. Rev. E*, 72:041921, 2005.

[7] T. Biben and C. Misbah. Tumbling of vesicles under shear flow within an advected-field approach. *Phys. Rev. E*, 67:031908, 2003.

[8] G. Boedec, M. Leonetti, and M. Jaeger. 3d vesicle dynamics simulations with a linearly triangulated surface. *J. Comput. Phys.*, 230(4):1020–1034, 2011.

[9] A. Bonito, R. H. Nochetto, and M. S. Pauletti. Parametric FEM for geometric biomembranes. *J. Comput. Phys.*, 229(9):3171–3188, 2010.

[10] S. C. Brenner and L. R. Scott. *The mathematical theory of finite element methods*. Springer, third edition, 2008.

[11] F. Brezzi and M. Fortin. *Mixed and hybrid finite element methods*. Springer, 1991.

[12] C. Bui, V. Lleras, and O. Pantz. Dynamics of red blood cells in 2d. *ESAIM Proc.*, 28:182–194, 2009.

[13] P. B. Canham. The minimum energy of bending as a possible explanation of the biconcave shape of the human red blood cell. *J. Theoret. Biol.*, 26:61–81, 1970.

[14] U. Clarenz, U. Diewald, G. Dziuk, M. Rumpf, and R. Rusu. A finite element method for surface restoration with smooth boundary conditions. *Computer Aided Geometric Design*, 21(5):427–445, 2004.

[15] G.-H. Cottet, E. Maitre, and T. Milcent. Eulerian formulation and level-set models for incompressible fluid-structure interaction. *Math. Model. Numer. Anal.*, 42:471–492, 2008.

[16] V. Doyeux, V. Chabannes, C. Prud'Homme, and M. Ismail. Siimulation pf vesicle using level set method solved by high order finite element. *ESAIM Proc.*, submited, 2012.

[17] Q. Du, C. Liu, R. Ryham, and X. Wang. Energetic variational approaches in modeling vesicle and fluid interactions. *Physica D*, 238:923–930, 2009.

[18] Q. Du, C. Liu, and X. Wang. A phase field approach in the numerical study of the elastic bending energy for vesicle membranes. *J. Comput. Phys.*, 198:450–468, 2004.

[19] Q. Du and J. Zhang. Adaptive finite element method for a phase field bending elasticity model of vesicle membrane deformation. *SIAM J. Ssci. Comput.*, 30(3):1634–1657, 2008.

[20] L. Formaggia and S. Perotto. New anisotropic *a priori* error estimates. *Numer. Math.*, 89:641–667, 2001.

[21] M. Fortin and R. Glowinski. *Augmented Lagrangian methods*. Elsevier, 1983.

[22] V. Girault and P. A. Raviart. *Finite element methods for the Navier-Stokes equations. Theory and algorithms*. Springer, 1986.

[23] G. H. Golub and C. F. van Loan. *Matrix computations*. The John Hopkins University Press, Baltimore, MD, USA, third edition, 1996.

[24] F. Hecht. *BAMG: bidimensional anisotropic mesh generator*, 2006. http://www.rocq.inria.fr/gamma/cdrom/www/bamg/eng.htm.

[25] W. Helfrich. Elastic properties of lipid bilayers: theory and possible experiments. *Z. Naturforsch*, 28(11):693–703, 1973.

[26] W. Huang. Metric tensors for anisotropic mesh generation. *J. Comput. Phys.*, 204:633–665, 2005.

[27] W. Huang and X. Li. An anisotropic mesh adaptation method for the finite element solution of variational problems. *Finite Elements in Analysis and Design*, 46:61–73, 2010.

[28] S. Hysing. A new implicit surface tension implementation for interfacial flows. *Int. J. Numer. Meth. Fluids*, 51(6):659–672, 2006.

[29] D. Jamet and C. Misbah. Toward a thermodynamically consistent picture of the phase-field model of vesicles: curvature energy. *Phys. Rev. E*, 78:031902, 2008.

[30] V. Kantsler and V. Steinberg. Transition to tumbling and two regimes of tumbling motion of a vesicle in shear flow. *Phys. Rev. Lett.*, 96:036001, Jan 2006.

[31] S. Keller and R. Skalak. Motion of a tank-treading ellipsoidal particle in a shear flow. *J. Fluid Mech.*, 120:27–47, 1982.

[32] Y. Kim and M.-C. Lai. Simulating the dynamics of inextensible vesicles by the penalty immersed boundary method. *J. Comput. Phys.*, 229(12):4840–4853, 2010.

[33] M. Kraus, W. Wintz, U. Seifert, and R. Lipowsky. Fluid vesicles in shear flow. *Phys. Rev. Lett.*, 77:3685–3688, Oct 1996.

[34] T. Krüger, F. Varnik, and D. Raabe. Efficient and accurate simulations of deformable particles immersed in a fluid using a combined immersed boundary lattice Boltzmann finite element method. *Comput. Math. Appl.*, 61(12):3485–3505, 2011.

[35] A. Laadhari, C. Misbah, and P. Saramito. On the equilibrium equation for a generalized biological membrane energy by using a shape optimization approach. *Phys. D*, 239:1568–1572, 2010.

[36] A. Laadhari, P. Saramito, and C. Misbah. Improving the mass conservation of the level set method. *C. R. Acad. Sci. Paris, ser. I*, 348:535–540, 2010.

[37] A. Laadhari, P. Saramito, and C. Misbah. Vesicle tumbling inhibited by inertia. *Phys. Fluids*, 24:031901, 2012.

[38] D.V. Le and S.T. Wong. A front-tracking method with catmull–clark subdivision surfaces for studying liquid capsules enclosed by thin shells in shear flow. *Journal of Computational Physics*, 230(9):3538–3555, 2011.

[39] L. Ma and W. S. Klug. Viscous regularization and r-adaptive remeshing for finite element analysis of lipid membrane mechanics. *J. Comput. Phys.*, 227(11):5816–5835, 2008.

[40] E. Maitre, T. Milcent, G.-H. Cottet, A. Raoult, and Y. Usson. Applications of level set methods in computational biophysics. *Math. Comput. Model.*, 49(11–12):2161–2169, 2009.

[41] S. Osher and J. A. Sethian. Front propaging with curvature-dependent speed: agorithms based on Hamilton-Jacobi formulations. *J. Comput. Phys.*, 79(12), 1988.

[42] Z.-C. Ou-Yang and W. Helfrich. Bending energy of vesicle membranes: general expressions for the first, second and third variation of the shape energy and applications to spheres and cylinders. *Phys. Rev. A*, 39(10):5280–5288, 1989.

[43] O. Pironneau. On the transport-diffusion algorithm and its applications to the Navier-Stokes equations. *Numerische Mathematik*, 38(3):309–332, 1982.

[44] C. Pozrikidis. Numerical simulation of the flow-induced deformation of red blood cells. *Annals of Biomedical Engineering*, 31:1194–1205, 2003.

[45] A. Rahimian, S. K. Veerapaneni, and G. Biros. Dynamic simulation of locally inextensible vesicles suspended in an arbitrary two-dimensional domain, a boundary integral method. *J. Comput. Phys.*, 229(18):6466–6484, 2010.

[46] R. Rusu. An algorithm for the elastic flow of surfaces. *Interfaces and Free Boundaries*, 7(3):229–239, 2005.

[47] S. A. Safran. *Statistical thermodynamics of surfaces, interfaces and membranes*. Frontier in physics, vol. 90. Addison-Wesley, Reading, USA, 1994.

[48] D. Salac and M. Miksis. A level set projection model of lipid vesicles in general flows. *J. Comput. Phys.*, 230:8192–8215, 2011.

[49] P. Saramito. *Efficient C++ finite element computing with Rheolef*. CNRS and LJK, 2011. http://www-ljk.imag.fr/membres/Pierre.Saramito/rheolef.

[50] U. Seifert. Configurations of fluid membranes and vesicles. *Adv. Phys*, 46:13–137, 1997.

[51] M. Sussman and E. Fatemi. An efficient, interface preserving level set redistancing algorithm and its application to interfacial incompressible fluid flow. *SIAM J. Sci. Comput*, 20(4):1165–1191, 1998.

[52] V. Vitkova, G. Coupier, M.-A. Mader, B. Kaoui, C. Misbah, and T. Podgorski. Tumbling of viscous vesicles in a linear shear field near a wall. *Journal of optoelectronics and advanced materials*, 11:1218–1221, 2009.

[53] P. M. Vlahovska, T. Podgorski, and C. Misbah. Vesicles and red blood cells in flow: From individual dynamics to rheology. *C. R. Physique*, 10:775–789, 2009.

[54] T. Williams and C. Keley. `gnuplot`: an interactive program, 2010. http://www.gnuplot.info.

[55] H. Zhao and E. S. G. Shaqfeh. The dynamics of a vesicle in simple shear flow. *Journal of Fluid Mechanics*, 674:578–604, 2011.

A Remark on the spontaneous curvature

Let denote by V_0 the area and by A_0 the perimeter of the vesicle Ω. Using as a characteristic length the radius R_0 of the circle having the same perimeter as $\partial\Omega$, the relation between the Lagrangian $\mathscr{L}$ and its dimensionless counterpart $\widetilde{\mathscr{L}}$ writes:

$$\widetilde{\mathscr{L}}(\widetilde{\Omega};\widetilde{\lambda},\widetilde{p}) = \frac{2R_0}{k_c}\,\mathscr{L}(\Omega;\lambda,p) = \int_{\partial\widetilde{\Omega}} \widetilde{H}^2\,\mathrm{d}\widetilde{s} + \widetilde{\lambda}\left(\int_{\partial\widetilde{\Omega}} \mathrm{d}\widetilde{s} - \widetilde{A}_0\right) + \widetilde{p}\left(\int_{\widetilde{\Omega}} \mathrm{d}\widetilde{x} - \widetilde{V}_0\right).$$

where $\widetilde{\lambda} = \dfrac{2}{k_c}\,\lambda R_0^2$ and $\widetilde{p} = \dfrac{2}{k_c}\,pR_0^3$. denote the dimensionless Lagrange multipliers. Recall that the reduced area $\gamma = \dfrac{V_0}{\pi} \times \left(\dfrac{2\pi}{A_0}\right)^2 = \dfrac{V_0}{\pi R_0^2}$. Then, for the dimensionless problem, the volume and area express $\widetilde{V}_0 = \dfrac{V_0}{R_0^2} = \pi\,\gamma$ and $\widetilde{A}_0 = \dfrac{A_0}{R_0} = 2\pi$. As a consequence, the reduced area γ is the unique dimensionless number of this problem, that characterizes the stationary shape of the vesicle: others parameters, such as k_c, has no effects.

Let us turn to the effect of the spontaneous curvature $H_0 \geq 0$: The Lagrangian writes:

$$\mathscr{L}(\Omega;\lambda,p) = \frac{k_c}{2}\int_{\partial\Omega} (H - H_0)^2\,\mathrm{d}s + \lambda\left(\int_{\partial\Omega} \mathrm{d}s - A_0\right) + p\left(\int_{\Omega} \mathrm{d}x - V_0\right). \quad (28)$$

From $(H - H_0)^2 = H^2 - 2HH_0 + H_0^2$, notice first that the last H_0^2 term is constant and thus, has no effects in the minimization problem. The only term that depend upon H_0 is the second one, involving $H_0 \int_{\partial\Omega} H\,\mathrm{d}s$. Using the general shape derivative analysis framework [35] with $f(H) = H$, we get, for any vector field $\mathbf{u}$:

$$\frac{\partial}{\partial\Omega}\left(\int_{\partial\Omega} H\,\mathrm{d}s\right)(\Omega).(\mathbf{u}) = \int_{\partial\Omega} 2K\,\mathbf{u}.\mathbf{n}\,\mathrm{d}s. \quad (29)$$

where K is the Gauss curvature of $\partial\Omega$. As $K = 0$ for two dimensional problems, the bidimensional vesicle equilibrium shape is independent of H_0 and depends only of the reduced area γ. The spontaneous curvature H_0 is only pertinent for three-dimensional problems.

B Remark on the redistanciation procedure

Let us consider the transport equation: $D_t\phi = \partial_t\phi + \mathbf{u}.\nabla\phi = 0$. Using the summation of repeated indices convention, we get: $\partial_i\phi\ \partial_i\partial_t\phi + \partial_i\phi\ \partial_i\left(u_j\partial_j\phi\right) = 0$ that writes also equivalently: $(1/2)\ \partial_t\left(|\nabla\phi|^2\right) + |\nabla\phi|^2(\mathbf{n}\otimes\mathbf{n}) : \mathbf{u} + \partial_i\phi.\partial_i\left(u_j\partial_j\phi\right)$. Remark that: $\partial_i\phi.\partial_i\left(u_j\partial_j\phi\right) = (1/2)\ u_j.\partial_j\left(\left(\partial_i\phi\right)^2\right) = (1/2)\ \mathbf{u}.\nabla\left(|\nabla\phi|^2\right) = |\nabla\phi|\mathbf{u}.\nabla(|\nabla\phi|)$. Then, we obtain: $D_t(|\nabla\phi|) = |\nabla\phi|\ \left(\mathrm{div}_s\,\mathbf{u} - \mathrm{div}\,\mathbf{u}\right)$. The density of the fluid is supposed to be constant, and the mass conservation leads to $\mathrm{div}\,\mathbf{u} = 0$. Moreover, in the context of vesicles, $\mathrm{div}_s\,\mathbf{u}$ since the membrane is supposed to be inextensible. Thus $D_t(|\nabla\phi|) = 0$. When $|\nabla\phi| = 1$ at $t = 0$, i.e. when ϕ is initially a distance function, this property is then preserved for all $t > 0$. When using the finite element approximation, we observe that this property is only approximately preserved, and thus, the redistancing procedure described in this paper is applied.

C Computation of the vesicle inclination

This appendix presents the computation of the angle θ of the shape Ω. Let (x_1, x_2) be the coordinate system for $\mathbb{R}^2$, containing the shape Ω and $\mathrm{d}x = \mathrm{d}x_1\mathrm{d}x_2$. The center of the vesicle is denoted by $(\bar{x}_1, \bar{x}_2)$, where $\bar{x}_1 = \left(\int_\Omega x_1\mathrm{d}x\right)/\mathrm{meas}(\Omega)$ and $\bar{x}_2 = \left(\int_\Omega x_2\mathrm{d}x\right)/\mathrm{meas}(\Omega)$. Let I be the inertia matrix of the vesicle relative to the vertical axis in $(\bar{x}_1, \bar{x}_2)$:

$$I_O = \begin{pmatrix} \int_\Omega \left(x_1 - \bar{x}_1\right)^2 \mathrm{d}x & \int_\Omega \left(x_1 - \bar{x}_1\right)\left(x_2 - \bar{x}_1\right)\mathrm{d}x \\ \int_\Omega \left(x_1 - \bar{x}_1\right)\left(x_2 - \bar{x}_1\right)\mathrm{d}x & \int_\Omega \left(x_2 - \bar{x}_1\right)^2 \mathrm{d}x \end{pmatrix}.$$

This symmetric matrix has two real eigenvalues and orthogonal eigenvectors. The inclination angle θ is defined as the angle between the eigenvector associated to the largest eigenvalue, and the x_1 axis.